PERGAMON

Journal of Structural Geology 24 (2002) 861–886

JOURNAL OF STRUCTURAL GEOLOGY

www.elsevier.com/locate/jstrugeo

Miocene extension and fault-related folding in the Highland Range, southern Nevada: a three-dimensional perspective

James E. Faulds[a,*], Eric L. Olson[b], Stephen S. Harlan[c,1], William C. McIntosh[d]

[a]*Nevada Bureau of Mines and Geology, University of Nevada, Reno, NV 89557, USA*
[b]*Department of Geology, University of Iowa, Iowa City, IA 52242, USA*
[c]*U.S. Geological Survey, P.O. Box 25046, MS 980, Federal Center, Denver, CO 80225, USA*
[d]*New Mexico Bureau of Mines, New Mexico Institute of Mining and Technology, Socorro, NM 87801, USA*

Received 7 August 2000; revised 20 January 2001; accepted 12 June 2001

Abstract

The Highland Range of southern Nevada contains a major anticline and syncline that constitute the westernmost segments of the Black Mountains accommodation zone in the highly extended Colorado River extensional corridor. The folds are defined by thick tilted sections of Miocene volcanic and sedimentary strata that accumulated immediately prior to and during regional extension. The folds are generally symmetrical, with interlimb angles that exceed 90°, subhorizontal hingelines, and steeply inclined axial surfaces. East- and west-dipping normal faults dominate the west- and east-tilted limbs of the folds, respectively. The limbs of the folds are parts of major half grabens. Tilt fanning within these half grabens and 15 new $^{40}Ar/^{39}Ar$ dates bracket major extension between about 16.5 and 11 Ma. Tilting of the opposing fold limbs occurred simultaneously and was contemporaneous with extension. The anticline and syncline are therefore interpreted as fault-related extensional folds produced by the partial, along-strike overlap of oppositely dipping normal-fault systems and attendant tilt-block domains. The anticline developed between overlapping listric normal faults that dip toward one another, including the east-dipping McCullough Range and west-dipping Keyhole Canyon faults. Each limb of the anticline is a rollover fold developed in the hanging wall of the inwardly dipping listric normal faults. The syncline formed between overlapping outwardly dipping listric faults, as adjacent fault blocks were tilted toward one another. The dominant folding style was fault-bend folding, with drag-folding and displacement-gradient folding playing subsidiary roles. The anticline and syncline significantly affected depositional patterns, with synextensional units, including two major ash-flow tuffs, thinning toward the anticlinal hinge and thickening toward the synclinal hinge. The Black Mountains accommodation zone is largely composed of intersecting northwest-trending anticlines and northeast-trending synclines, both occurring at a variety of scales depending on the amount of overlap between the opposing normal-fault systems. This three-dimensional geometry contrasts with the typical style of folding in contractional settings and may characterize extensional accommodation zones that include the partial along-strike overlap of multiple, oppositely dipping normal faults. The folds in the Highland Range serve as well-exposed analogues of similar features in hydrocarbon-rich areas of submerged continental margins.

Keywords: Extension; Accommodation Zone; Basin and Range Province; Folding; Nevada

1. Introduction

Anticlines and synclines are fundamental features within extended terranes. Folds in extensional orogens may result from (a) movement on listric normal faults (i.e. rollover or reverse drag folds) (e.g. Hamblin, 1965; Groshong, 1989, 1994; Dula, 1991; Xiao and Suppe, 1992; Schlische, 1993), (b) displacement gradients on normal faults (e.g. Schlische, 1992, 1995; Janecke et al., 1998), (c) along-strike overlap of oppositely dipping normal faults within accommodation zones (e.g. Rosendahl, 1987; Morley et al., 1990; Faulds and Varga, 1998), and (d) isostatically induced flexures in the footwalls of major normal faults (e.g. Spencer, 1984; Wernicke and Axen, 1988). Fault-related folds in extended terranes are especially abundant in the belts of overlapping, oppositely dipping normal-faults (i.e. accommodation or transfer zones) and have been observed in the East African rift (Rosendahl, 1987; Scott and Rosendahl, 1989; Ebinger, 1989; Flannery and Rosendahl, 1990; Morley et al., 1990), Gulf of Suez (Colletta et al., 1988; Patton et al., 1994), North Sea (Morley et al., 1990), the Basin and Range province (Stewart, 1980; Faulds, 1996; Kruger et al.,

* Corresponding author. Tel.: +1-775-784-6691; fax: +1-775-784-1709.
E-mail address: jfaulds@unr.edu (J.E. Faulds).
[1] Now at Department of Geography, George Mason University, Fairfax, VA 22030, USA.

0191-8141/02/$ - see front matter
PII: S0191-8141(01)00116-X

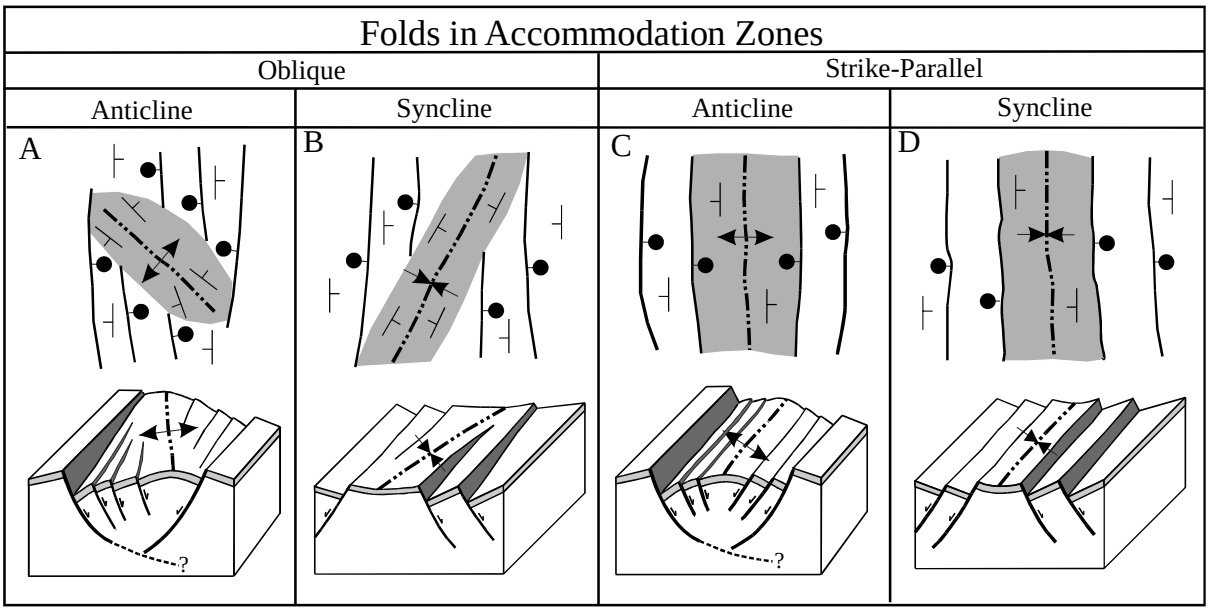

Fig. 1. Schematic block diagrams of fault-related folds in extensional accommodation zones (modified slightly from Faulds and Varga, 1998). See text for explanation. (a) Oblique anticline. (b) Oblique syncline. (c) Strike-parallel anticline. (d) Strike-parallel syncline.

1998; Faulds and Varga, 1998), and many other extended terranes.

The geometry of these folds is typically controlled by the dip direction of, and magnitude of along-strike overlap between, oppositely dipping normal faults (Faulds and Varga, 1998). Anticlines develop between listric normal faults that dip toward one another. Each limb of the anticline is a rollover fold developed in the hanging wall of one of the listric normal faults (Fig. 1). Synclines form between outwardly dipping listric faults, as adjacent fault blocks are tilted toward one another, possibly through a combination of reverse drag (e.g. Hamblin, 1965) and footwall uplift. Depending on the amount of along-strike overlap between the oppositely dipping fault systems and the

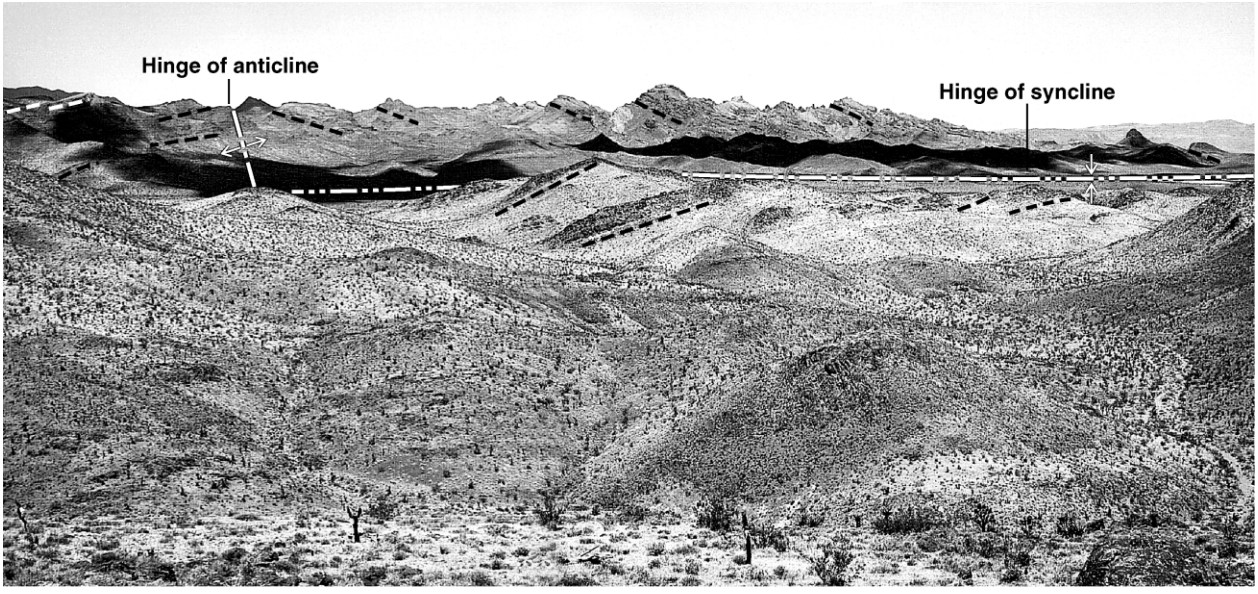

Fig. 2. Anticline and syncline in the Highland Range looking north. Black and white dashed lines are form-lines illustrating the approximate dip of strata. Several small west-tilted fault blocks comprise the low ridges in the middle ground. In descending order, strata within these blocks are composed of the 15.0 Ma tuff of Mount Davis (cliff-forming capping unit), 15.2 Ma tuff of Bridge Spring, and basaltic trachyandesite lavas of the volcanics of the Highland Range (darker tones in foreground). The limbs of the anticline are well exposed in the high ridges on the horizon and consist primarily of ~18–16 Ma basaltic trachyandesite and trachyandesite lavas within the volcanics of the Highland Range. The view on the horizon is approximately 7 km across. Both the anticline and syncline terminate at the intersection of their hingelines behind the small hill at left center. It is noteworthy that the anticline forms a broad topographic high, whereas the syncline marks a topographic low. This photo was taken about 1 km southeast of $^{40}Ar/^{39}Ar$ sample locality J (east-central part of map area, Fig. 4).

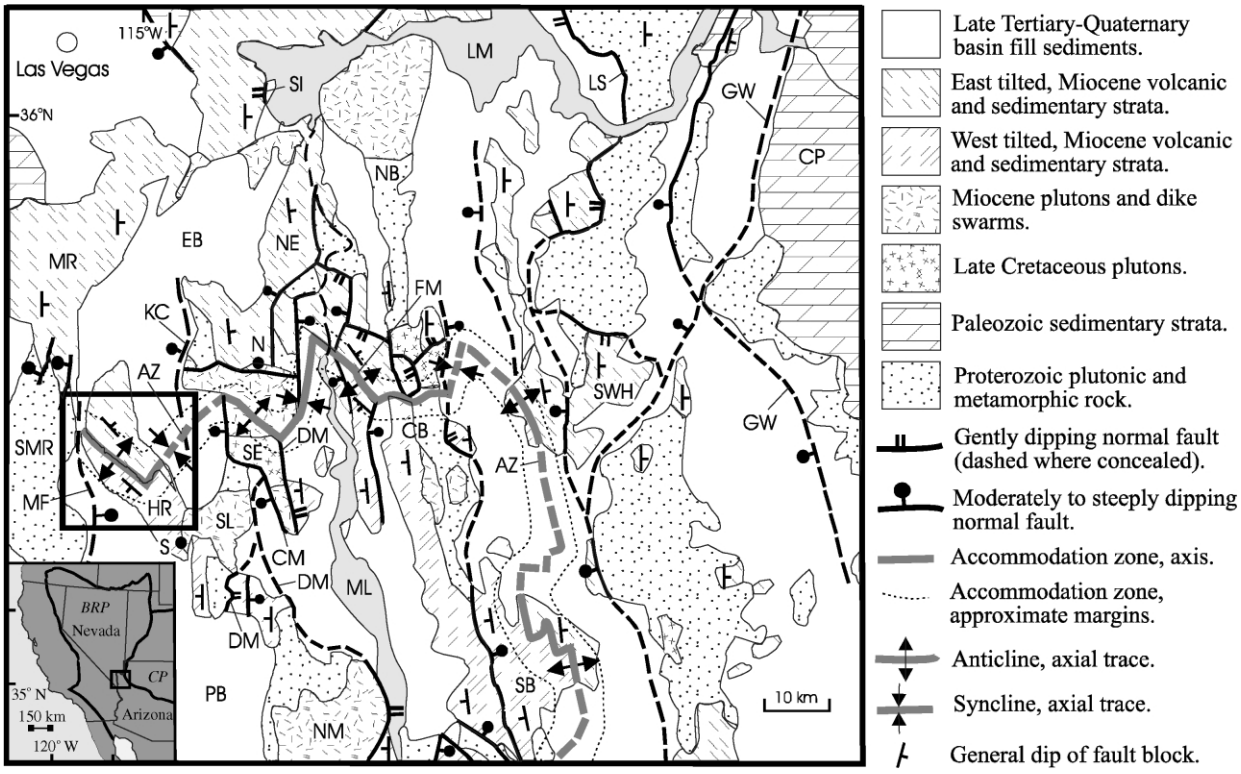

Fig. 3. Generalized geologic map of the northern Colorado River extensional corridor. The box surrounds the study area in the Highland Range, which is shown in more detail in Fig. 4. The margins of the accommodation zone correspond to the extent of multiple, overlapping east- and west-dipping normal faults of the Lake Mead and Whipple domains, respectively, and/or the area in which tilts begin decreasing appreciably toward the axis of the zone. The axis of the accommodation zone (AZ) marks the area in which tilt directions reverse and thus corresponds, in many cases, to the axial traces of the anticlines and synclines that comprise much of the zone. BRP, Basin and Range province (insert); CB, central Black Mountains; CM, Copper Mountain fault; CP, Colorado Plateau; DM, Dupont Mountain fault; EB, Eldorado basin; FM, Fire Mountain anticline; GW, Grand Wash fault zone; HR, Highland Range; KC, Keyhole Canyon fault; LM, Lake Mead; LS, Lakeside Mine–Salt Spring Wash fault; MF, McCullough Range fault; ML, Lake Mohave; MR, McCullough Range; N, Nelson, Nevada; NB, northern Black Mountains; NE, northern Eldorado Mountains; NM, Newberry Mountains; PB, Piute basin; SB, southern Black Mountains; S, Searchlight, Nevada; SE, southern Eldorado Mountains; SI, Saddle Island fault; SL, Searchlight pluton; SMR, southern McCullough Range; SWH, southern White Hills.

severity of the displacement gradient, these folds may trend parallel, oblique, or transverse to the strike of the normal faults. Strike-parallel folds develop between oppositely dipping normal faults or systems of faults characterized by complete along-strike overlap and minimal displacement gradients. Oblique folds form between en échelon normal faults or fault systems characterized by partial along-strike overlap and/or significant displacement gradients (Fig. 1).

Although these folds have been widely recognized, relatively few have been studied in detail (see discussion in Janecke et al., 1998). Comprehensive three-dimensional analysis of these folds is important for elucidating their geometry, kinematic development, and economic significance and for constraining the three-dimensional strain field in extended terranes. In the latter case, an important question is whether these folds are purely extensional strain features or instead the result of localized shortening associated with diametric lateral motions of individual fault blocks or large extensional allochthons above oppositely dipping major normal faults (e.g. detachment faults). From an economic standpoint, such folds can significantly influence the distribution of sedimentary facies (e.g. Scott and Rosendahl, 1989; Gawthorpe and Hurst, 1993; May and Russell, 1994; Russell and Snelson, 1994) and can also form structural and sedimentary traps for hydrocarbons, which may account for the affinity of large oil fields on passive continental margins with extensional accommodation zones (e.g. Etheridge et al., 1988; Morley et al., 1990).

In this paper, we examine a relatively well-exposed Tertiary anticline and syncline, of presumed extensional origin, in Miocene rocks of the Highland Range in southern Nevada (Fig. 2). The Highland Range lies within the western part of the northern Colorado River extensional corridor (Howard and John, 1987; Faulds et al., 1990), a highly extended portion of the Basin and Range province in southern Nevada and northwest Arizona. Here, we report the results of detailed geologic mapping, structural analysis, and $^{40}Ar/^{39}Ar$ geochronology, which were employed to document the timing of deformation and the three-dimensional geometry, age, and origin of the folds.

2. General geologic setting

The highly extended northern Colorado River extensional corridor (Fig. 3) is bounded by the unextended Colorado Plateau to the east, relatively unextended ranges to the west (e.g. Spring Range), and right-lateral Las Vegas Valley shear zone and left-lateral Lake Mead fault system to the north (Weber and Smith, 1987; Faulds et al., 1990). In his classic study of the northern Eldorado Mountains, Anderson (1971, 1977, 1978) was the first to carry out detailed geologic mapping and describe large-magnitude extension in the region. On the basis of K/Ar dating of variably tilted units in growth-fault basins, major extension was constrained to middle Miocene time (Anderson et al., 1972). Anderson (1971) also provided some of the first detailed descriptions of regionally extensive volcanic units, including the Patsy Mine Volcanics, tuff of Bridge Spring, and Mount Davis Volcanics. These units have since become important time-stratigraphic markers throughout the northern Colorado River extensional corridor, including the Highland Range. The north-trending Highland Range lies near the western margin of the extensional corridor about 25 km southwest of the northern Eldorado Mountains (Fig. 3).

Recent studies have shown that magmatism and extension migrated northward through the corridor in early to middle Miocene time (Glazner and Bartley, 1984; Gans et al., 1989; Faulds et al., 1994, 1999; Smith and Faulds, 1994). Voluminous outpourings of volcanic rock occurred just prior to and during extension. Thus, the corridor is dominated by complex arrays of fault blocks containing 2–5-km-thick sections of Miocene volcanic rock and associated clastic sediments (e.g. Anderson, 1971; Turner and Glazner, 1990; Duebendorfer and Wallin, 1991; Faulds et al., 1995; Duebendorfer and Sharp, 1998; Gans and Bohrson, 1998). Appreciable tilting of fault blocks has exposed thick crustal sections in both the Lake Mead (Fryxell et al., 1992) and Lake Mohave areas (Faulds et al., 1995, 1998) (Fig. 3).

The northern part of the corridor consists of two discrete domains of oppositely dipping normal faults and associated tilt block domains. West-tilted fault blocks and east-dipping normal faults dominate in the south, whereas east-tilted fault blocks and west-dipping normal faults prevail in the north. These domains are referred to as the Whipple and Lake Mead domains, respectively (Spencer and Reynolds, 1989).

The Black Mountains accommodation zone separates the two domains and spans nearly the entire extensional corridor (Fig. 3). It is a 5–15-km-wide belt of overlapping, oppositely dipping normal faults (Faulds et al., 1990, 1992). In the Whipple domain, more than 100 km south of the accommodation zone, a system of east-dipping detachment faults is well documented in the Sacramento, Chemehuevi, and Whipple Mountains metamorphic core complexes (Davis et al., 1980; Howard and John, 1987; Davis and Lister, 1988; Yin and Dunn, 1992; John and Foster, 1993; Campbell and John, 1996). This system continues northward into the northern Colorado River extensional corridor and possibly terminates within the accommodation zone (Faulds et al., 1996). Conversely, west-dipping detachment faults may floor the Lake Mead domain (Wernicke, 1985; Wernicke and Axen, 1988; Duebendorfer et al., 1990; Fryxell et al., 1992; Duebendorfer and Sharp, 1998) and die out southward within the accommodation zone. Thus, oppositely dipping detachment faults may underlie the Whipple and Lake Mead domains and interact within the Black Mountains accommodation zone.

Detailed geologic mapping, structural analysis, and $^{40}Ar/^{39}Ar$ geochronology have demonstrated coeval extension in the northern Whipple (north of the southern tip of Nevada) and Lake Mead domains, with the major episode bracketed between about 16 and 9 Ma (Faulds et al., 1994, 1995, 1999). Thus, the oppositely dipping normal-fault systems and possibly the subjacent opposing detachment faults were active contemporaneously within the Black Mountains accommodation zone (Faulds et al., 1990), which implies that displacement transfer mechanisms at the crustal scale can be studied within this region.

The Black Mountains accommodation zone is characterized by a series of northwest-trending anticlines and northeast-trending synclines (Faulds, 1994), both of which are oblique to the east–northeast-trending regional extension direction (e.g. Anderson et al., 1994). Although the general character of the Black Mountains accommodation zone has been described (Faulds et al., 1990; Faulds and Varga, 1998), the anticlines and synclines in the zone have not been addressed in any detail. The Highland Range contains the two westernmost folds within the accommodation zone. These folds developed between several overlapping east- and west-dipping normal faults in the Whipple and Lake Mead domains, respectively; most notably, the McCullough Range and Keyhole Canyon faults (Fig. 3).

3. Highland Range

3.1. Structural framework

The southeastern Highland Range constitutes the upper part of a large steeply west-tilted fault block, the bulk of which resides in the neighboring southern Eldorado Mountains (Fig. 3). This fault block exposes a crustal section that approaches 15 km in thickness and includes the 10 + -km-thick, 16.5 Ma Searchlight pluton (Miller et al., 1995, 1998; Faulds et al., 1996, 1998; Bachl, 1997) in the southern Eldorado Mountains and at least 3 km of volcanic strata in the southeastern Highland Range (Faulds and Bell, 1999). The block is tilted nearly 90° and therefore reveals a cross-section of the upper crust. It is bounded by the east-dipping McCullough Range fault on the west and the gently east-dipping Dupont Mountain fault on the east (Fig. 3). In addition, several major east-dipping normal faults cut the

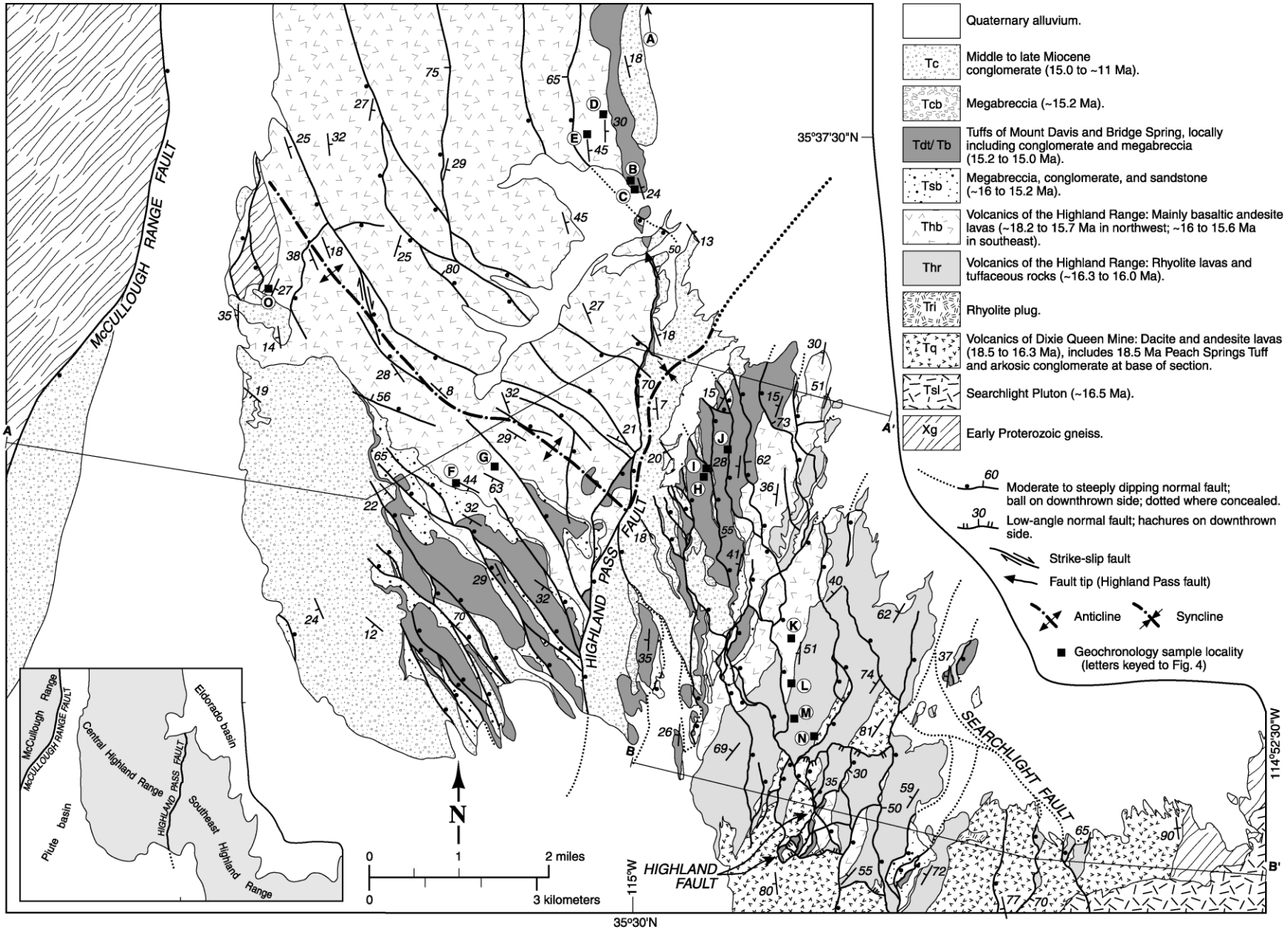

Fig. 4. Generalized geologic map of the central and southeastern Highland Range, Nevada (from Davis, 1984; Olson, 1996; Faulds and Bell, 1999). Circled letters indicate $^{40}Ar/^{39}Ar$ sample locations (see Table 1; Fig. 8). Cross-sections A–A′ and B–B′ are shown in Fig. 5.

block in the southeastern Highland Range (e.g. Highland and Searchlight faults; Fig. 4).

The McCullough Range fault probably links southward with a breakaway fault, described by Spencer (1985), that separates highly extended crust in the Colorado River extensional corridor from much less extended terrane to the west. Spencer (1985) surmised that the breakaway fault is part of the major east-dipping detachment system related to uplift and tectonic denudation of the Sacramento, Chemehuevi, and Whipple Mountains metamorphic core complexes. Similarly, Turner and Glazner (1990) concluded that major east-dipping normal faults in the Castle Mountains, which lie directly west of the Piute basin to the south of the McCullough Range, are part of the same breakaway system. The Dupont Mountain fault also continues southward and appears to connect with major east-dipping detachment faults on the east flank of the Sacramento and Chemehuevi Mountains.

Both the Dupont Mountain and McCullough Range faults terminate northward in the Black Mountains accommodation zone (Fig. 3). Between the latitude of Searchlight, Nevada, and the axis of the accommodation zone, displacement on the Dupont Mountain fault decreases from more than 12 km to about 1 km concomitant with a decrease in offset on the McCullough Range fault from about 8 km to less than 1 km. Both faults terminate in the southernmost part of the Lake Mead domain, where they form major antithetic faults to the predominant west-dipping normal-fault system (Fig. 3). The northward decrease in displacement and ultimate termination of the Dupont Mountain and McCullough Range faults may reflect the termination of the east-dipping detachment system in the Whipple domain and a corresponding transfer of strain to a west-dipping detachment system in the Lake Mead domain.

As displacement on major east-dipping normal-faults, including the McCullough Range and Highland Pass faults, decreases northward, west dips in the southeast Highland Range give way to east dips to the north across a broad, well-exposed northwest-trending anticline and a northeast-trending syncline (Figs. 2 and 4). Accordingly, the large west-tilted fault block of the southern Eldorado Mountains and southeastern Highland Range terminates northwestward in the central Highland Range. The west limb of the anticline is interpreted as a rollover fold in the hanging wall of the McCullough Range fault. The anticline in the central Highland Range is the westernmost segment of the Black Mountains accommodation zone.

Two major west-dipping normal faults, the Keyhole Canyon and Copper Mountain faults, bound the central and southern Eldorado basin on the east and accommodated much of the east-tilting in the central and northern Highland Range. The Keyhole Canyon fault borders a large steeply east-tilted fault block in the northern Eldorado Mountains on the west and the central part of the Eldorado basin on the east (Fig. 3). It probably continues southward into the southern Eldorado basin about 10 km east of the northern and central Highland Range but is covered by late Tertiary and Quaternary sediments. The west-dipping Copper Mountain fault, which may link northward with the Keyhole Canyon fault across a left step in the Eldorado Mountains, juxtaposes late Tertiary–Quaternary alluvium within the southern Eldorado basin against the uplifted crystalline terrane of the central and southern Eldorado Mountains. It is locally exposed on the west flank and within the southernmost part of the southern Eldorado Mountains. The Copper Mountain fault loses displacement southward in the southern Eldorado Mountains, where it becomes a major antithetic west-dipping normal fault in the northern Whipple domain (Fig. 3). The Keyhole Canyon and Copper Mountain faults are part of the west-dipping normal-fault system in the northern Eldorado Mountains that Anderson (1971) documented as accommodating large-magnitude thin-skinned extension.

Proposed west-dipping detachment faults in the Lake Mead domain (e.g. Wernicke, 1985; Wernicke and Axen, 1988; Duebendorfer et al., 1990) may be related to the major west-dipping normal faults near the Highland Range. For example, the Saddle Island fault in the western Lake Mead area, which has been interpreted as a major west-dipping detachment fault (Duebendorfer et al., 1990), may be kinematically linked to the west-dipping normal-fault system in the northern Eldorado Mountains, as well as the Keyhole Canyon and Copper Mountain faults. However, the probable breakaway for this west-dipping detachment system is the Grand Wash fault zone, which lies far to the east of the Highland Range along the western margin of the Colorado Plateau (Fig. 3).

As with the entire Black Mountains accommodation zone, the Highland Range may therefore straddle the boundary between two oppositely dipping detachment systems. Major east- and west-dipping normal faults that overlap in the vicinity of the Highland Range may sole into these opposing detachment faults at depth. The folds within the Highland Range could therefore be attributed to localized shortening associated with convergent motion of discrete extensional allochthons above opposing detachment faults (Faulds et al., 1990). Alternatively, they may simply be products of extensional strain related to displacement transfer between the tips of overlapping, oppositely dipping upper-crustal normal-fault systems. A three-dimensional perspective, incorporating both along-strike and cross-sectional perspectives, is needed to assess the origin of these folds.

3.1.1. Anticline

The 10-km-long northwest-trending anticline is the most prominent structural feature within the central Highland Range. As first noted by Davis (1984), it is defined by tilted Miocene volcanic and sedimentary strata (Figs. 2 and 4). The anticline is an open (interlimb angle between 90 and 170°), generally symmetrical, parallel fold, with a subhorizontal (plunge $<10°$) hingeline and upright (dip

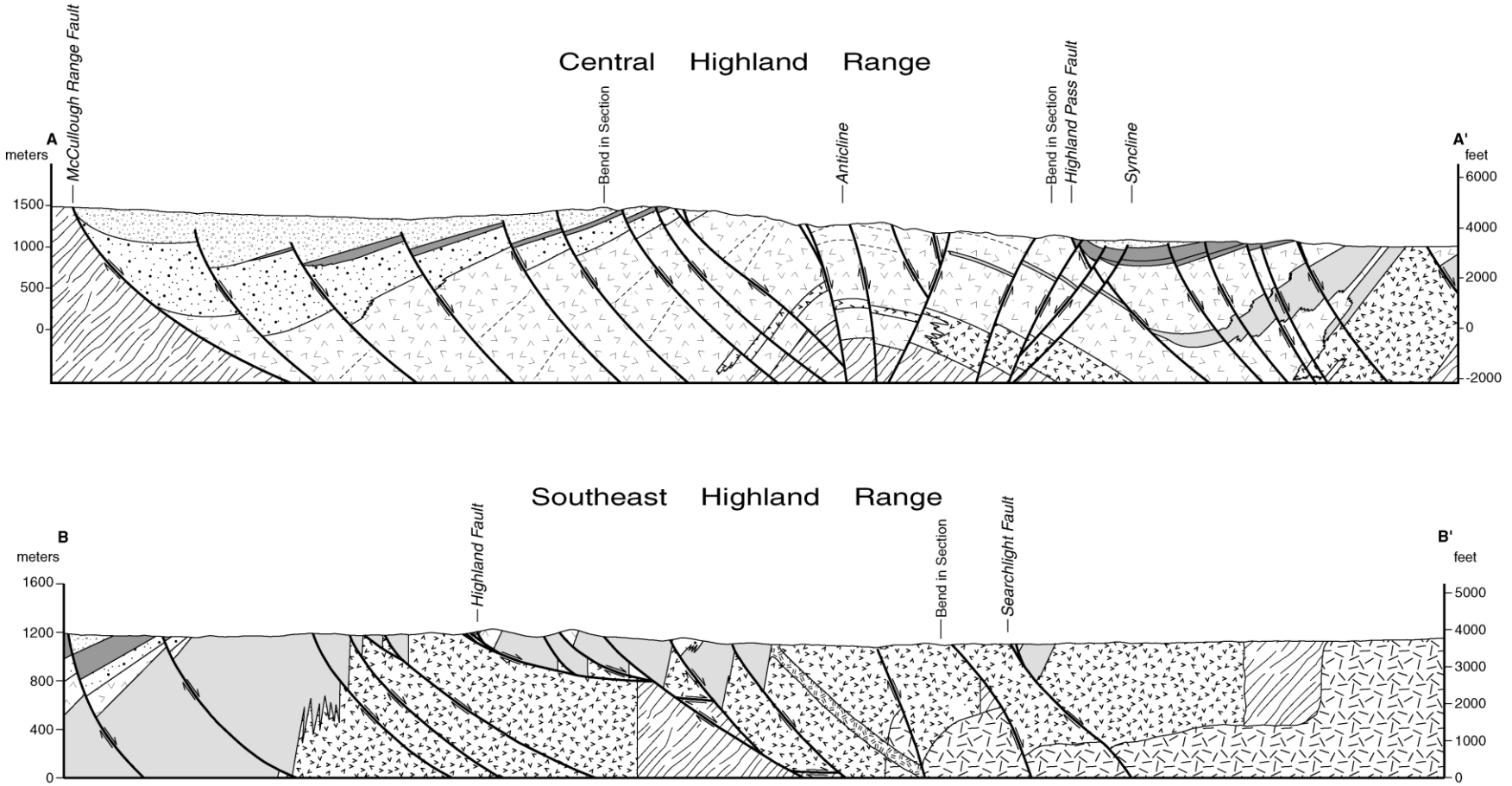

Fig. 5. Cross-sections of the central (A–A′) and southeastern (B–B′) Highland Range. The location of, and lithologic patterns used within, the cross-sections are shown in Fig. 4. Quaternary units shown in Fig. 4 were omitted from the cross-sections to enhance clarity of bedrock relations. (a) Note that both anti-listric (i.e. convex upward) and listric normal faults accommodate changes in tilt magnitude near the hinge zones of the folds. Listric faults dominate in the syncline, whereas anti-listric faults are common near the hinge zone of the anticline. The steep west limb of the syncline in this profile is attributed to normal drag along the northern tip of the Highland Pass fault. Directly north of this profile, the syncline broadens (i.e. interlimb angle increases) and becomes more symmetric as the Highland Pass fault terminates. (b) Note that the gently dipping Highland fault is cut by younger, more steeply dipping normal faults. This part of the Highland Range constitutes the upper part of a steeply west-tilted fault block that continues eastward into the southern Eldorado Mountains and approaches 15 km in thickness.

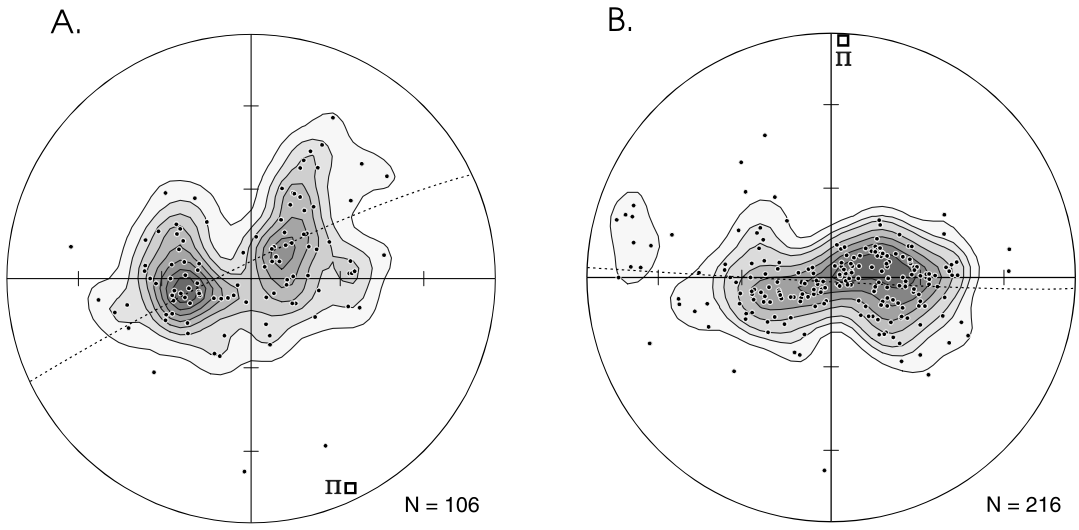

Fig. 6. Lower-hemisphere equal-area stereographic projections of poles to layering and bedding for the anticline (a) and syncline (b). Density contour plots indicate the percent of data per 1% area. *N*, number of measurements (shown as dots). (a) Poles from the anticline define a π circle (dashed great circle), which indicates an average fold axis (small open box labeled π) plunging 5° to the south–southeast (~154°), which is slightly oblique to the more northwesterly trend of the axial trace of the fold shown in Fig. 4. Contour intervals are 0, 2, 4, 6, 8, 10, 12, and 14% per 1% area. (b) Poles from the syncline define a π circle that indicates a gently (~2°) north-plunging fold axis. Much of the syncline trends northeast, but these data are skewed by the well-exposed northerly trending, southern part of the syncline that roughly parallels the Highland Pass fault (Fig. 4). Contour intervals are 0, 2, 4, 8, 12, 16, and 20% per 1% area.

>80°) axial surface (cf. Fleuty, 1964; Ramsay, 1967) (Fig. 5). At exposed levels, the interlimb angle is about 105°. The anticline trends N35°W to N50°W and plunges about 5° southeast (Fig. 6a). Northwesterly strikes characterize tilted strata near the anticline, especially on the southwest limb, and contrast with the predominant northerly striking structural grain of Miocene rocks within the northern Colorado River extensional corridor. The anticline terminates to the

Fig. 7. Syncline separating the central and southeastern parts of the Highland Range looking southeast. The prominent east-dipping hogback in the foreground and trending off to the right consists primarily of the 15.0 Ma tuff of Mount Davis and isolated exposures of the 15.2 Ma tuff of Bridge Spring, which overlie basaltic trachyandesite lavas of the volcanics of the Highland Range. All of these units are also exposed on the east limb of the syncline in the west-tilted ridges in the background (see dashed, black form-lines). On each limb of the syncline, the tuffs of Mount Davis and Bridge Spring thicken toward the hinge zone. $^{40}Ar/^{39}Ar$ sample locality D was collected from the ridge (partly in shadow) in the foreground (see northeast part of Fig. 4). It is noteworthy that the syncline forms a broad topographic swale in contrast to the high-relief (synclinal) accommodation zones noted by Rosendahl (1987) in the East African rift.

northwest near the northern tip of the McCullough Range fault (Fig. 3) and to the southeast against the Highland Pass fault at the intersection with the syncline (Fig. 4). Near the southeast terminus, the anticline becomes asymmetric, as the east limb dips more steeply near the Highland Pass fault. The southeast terminus is marked by the topographic and structural low of the synclinal hinge zone, which also constitutes the approximate boundary between the central and southeastern structural and lithologic domains of the Highland Range (Fig. 4, see insert).

Directly west of the northwest end of the anticline, near an isolated exposure of Proterozoic gneiss (Fig. 4), strata are deformed into two small-amplitude secondary folds (not shown in Fig. 4) as west dips give way northward to east dips. Just to the north of the inferred tip of the McCullough Range fault, Miocene strata within the McCullough Range dip gently to moderately eastward toward the Eldorado basin (DeWitt et al., 1989). Thus, a major east-dipping normal fault is not required between the northern Highland Range and east flank of the McCullough Range (Fig. 3).

3.1.2. Syncline

The syncline separating the southeastern and central parts of the Highland Range trends north to northeast and plunges gently south near its southern end and gently northeast farther north (Figs. 3, 4, and 6b). It was first documented by Olson (1996). The syncline ends to the southwest at the intersection with the anticline. The east limb of the syncline corresponds to the upper part of the large aforementioned west-tilted faulted block that comprises much of the southern Eldorado Mountains and southeastern Highland Range. Much of the syncline is buried beneath the Eldorado basin, but its southwestern part is well exposed. It is defined by gently dipping middle to late Miocene conglomerate within the hinge zone and oppositely tilted ridges of middle Miocene ash-flow tuffs on the limbs (Figs. 4 and 7). The syncline is an open, asymmetric to symmetric, parallel fold, with a steeply inclined (60–80° dip) axial surface and subhorizontal (plunge $<10°$) hingeline (Fig. 5) (cf. Fleuty, 1964; Ramsay, 1967). The interlimb angle is about 100–125° at exposed levels. The steep east dip ($\sim 70°$) of the west limb of the syncline decreases to the north; accordingly, the syncline becomes more symmetric to the northeast. The syncline projects northeastward into the southern part of the Eldorado basin, where it is largely buried by late Tertiary–Quaternary alluvium. It ultimately links northeastward with an anticline in the central Eldorado Mountains (Fig. 3).

3.1.3. Geometry and kinematics of faults

The southeastern Highland Range, which includes the eastern, west-tilted limb of the syncline, is dominated by northerly striking, east-dipping normal faults that cut Miocene strata (Olson, 1996; Faulds and Bell, 1999). Good kinematic indicators, such as rough facets and Riedel shears (cf. Angelier et al., 1985), are sparse but generally indicate dominantly normal slip. Normal separation of stratigraphic units is ubiquitous. The strike of the faults and dominance of normal slip are compatible with the east–northeast-trending regional extension direction established by Anderson et al. (1994) in the northern part of the extensional corridor. Offset on most faults is less than 500 m, but the Highland Pass, Highland, and Searchlight faults all accommodated several kilometers of normal displacement (Figs. 4 and 5b), as evidenced by stratigraphic throw across the faults.

Within the anticline in the central Highland Range, faults generally dip steeply and strike northwest (Figs. 4 and 5) (Davis, 1984). Most faults accommodated normal displacement of generally less than 250 m. The northwest-striking faults on the west-tilted limb of the anticline typically dip steeply northeast and appear to merge with the northerly striking Highland Pass fault to the southeast. On the shared east-tilted limb of the anticline and syncline, faults generally dip steeply westward. Both east- and west-dipping normal faults are found in the hinge zones of the folds, especially in the southern wedge-shaped tip of the east-tilted domain near the intersection of the anticline and syncline (Fig. 4). Crosscutting relationships between the oppositely dipping normal-fault sets are not consistent and are commonly ambiguous.

The Highland Pass fault separates a domain of northwest-striking faults in the central Highland Range from northerly striking faults to the southeast. Both the north- and northwest-striking faults primarily accommodated normal slip. This suggests that the three-dimensional strain field near the hinge zone of the anticline differed slightly from that to the southeast and in much of the northern part of the extensional corridor.

It is important to note that major reverse faults were not observed in the central Highland Range. Analysis of several faults, mapped by Davis (1984) as reverse faults, revealed kinematic indicators indicative of either strike-slip or normal movement. Only a few minor, steeply dipping reverse-separation faults were observed; these probably resulted from tilting of originally antithetic normal faults (e.g. west tilting of an originally steep, west-dipping normal fault). Thus, horizontal shortening was not a significant component of the strain field. However, several minor northwest- to north–northwest-striking dextral faults and west- to west–northwest-striking sinistral faults were observed within or near the hinge zone of the anticline.

The most significant faults in the vicinity of the Highland Range are the east-dipping McCullough Range fault and west-dipping Keyhole Canyon and Copper Mountain faults. The McCullough Range fault juxtaposes the west-tilted Miocene strata of the southwestern part of the Highland Range against Early Proterozoic basement of the southern McCullough Range (Figs. 3–5a). The southern part of the McCullough Range does not appear to be significantly tilted. The differential tilt between the southern McCullough Range and Highland Range indicates a listric geometry for

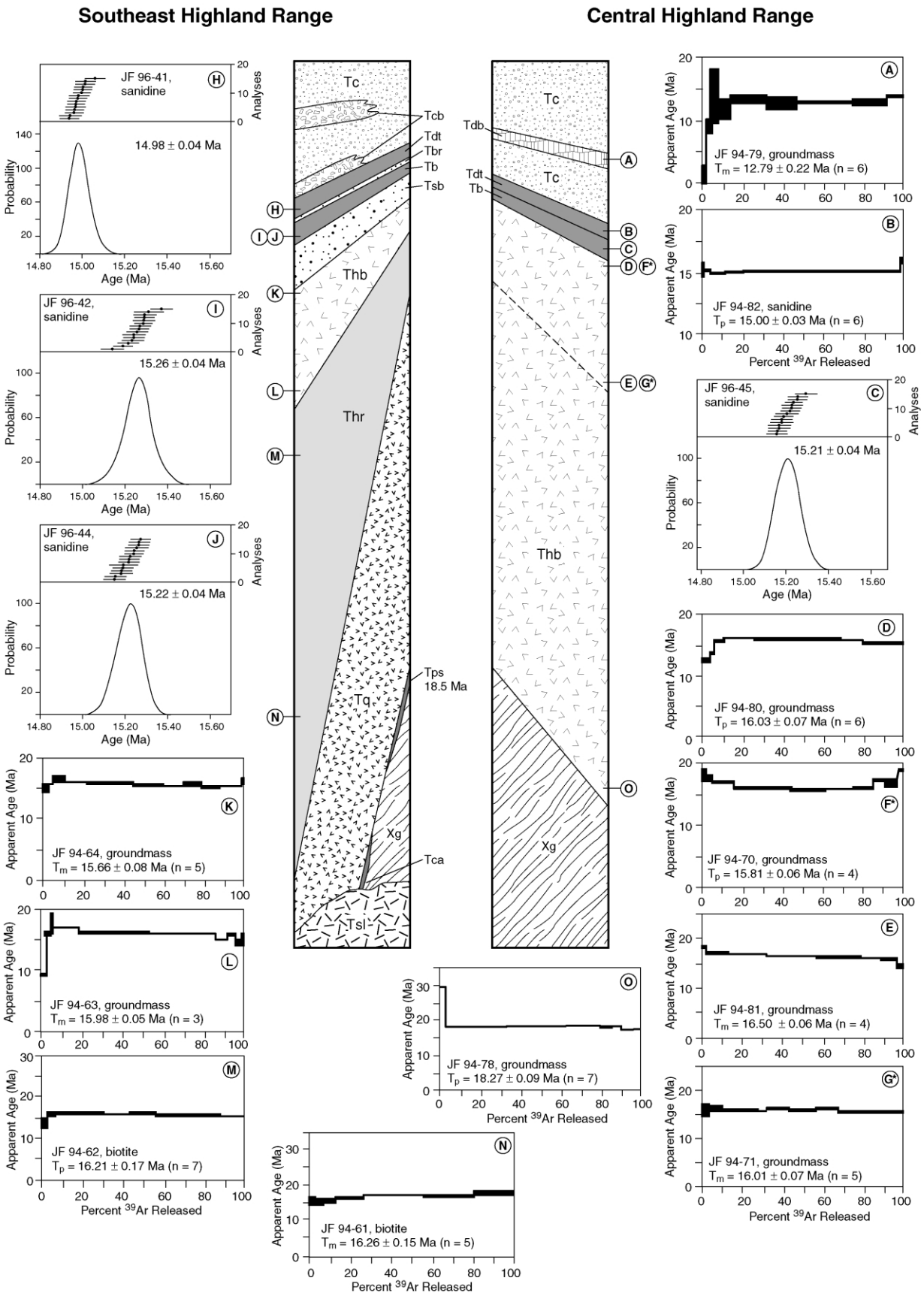
Southeast Highland Range
Central Highland Range
JF 96-41, sanidine
14.98 ± 0.04 Ma
JF 96-42, sanidine
15.26 ± 0.04 Ma
JF 96-44, sanidine
15.22 ± 0.04 Ma
Probability
Analyses
Age (Ma)
Tc
Tcb
Tdt
Tbr
Tb
Tsb
Thb
Thr
Tq
Tps
18.5 Ma
Xg
Tca
Tsl
Tdb
JF 94-64, groundmass
Tm = 15.66 ± 0.08 Ma (n = 5)
JF 94-63, groundmass
Tm = 15.98 ± 0.05 Ma (n = 3)
JF 94-62, biotite
Tp = 16.21 ± 0.17 Ma (n = 7)
JF 94-61, biotite
Tm = 16.26 ± 0.15 Ma (n = 5)
JF 94-78, groundmass
Tp = 18.27 ± 0.09 Ma (n = 7)
JF 94-79, groundmass
Tm = 12.79 ± 0.22 Ma (n = 6)
JF 94-82, sanidine
Tp = 15.00 ± 0.03 Ma (n = 6)
JF 96-45, sanidine
15.21 ± 0.04 Ma
JF 94-80, groundmass
Tp = 16.03 ± 0.07 Ma (n = 6)
JF 94-70, groundmass
Tp = 15.81 ± 0.06 Ma (n = 4)
JF 94-81, groundmass
Tm = 16.50 ± 0.06 Ma (n = 4)
JF 94-71, groundmass
Tm = 16.01 ± 0.07 Ma (n = 5)
Apparent Age (Ma)
Percent 39Ar Released

Table 1
$^{40}Ar/^{39}Ar$ isotopic age determinations, Highland Range, Nevada. Notes: Samples A through O correspond to letters showing locations in Fig. 5. Locations: CH-AE, central Highland Range, east limb of anticline; CH-AW, central Highland Range, west limb of anticline; CH-b, central Highland Range, base of Miocene section; SHR, southeastern Highland Range. Unit: Tdb, basalt lava in Mount Davis Volcanics; Tdt, tuff of Mount Davis; Tb, tuff of Bridge Spring; Thb, basaltic trachyandesite lava; Thr, rhyolite lava; Tha, trachyandesite lava. Material: bt, biotite; gm, groundmass concentrate; sd, sanidine. *n* is number of heating steps or crystals used to calculate weighted mean age. Sources: 1. U.S. Geological Survey, Denver: weighted mean or plateau ages from resistance-furnace, incremental-heating age spectra. Sample irradiation: sanidine and biotite separates, and groundmass concentrates in foil packets in SiO_2 tubes, interspersed with MMhb-1 monitors (520.4 Ma; Samson and Alexander, 1987), were irradiated in central thimble of U.S. Geological Survey TRIGA Reactor, Denver. Instrumentation: Mass Analyzer Products 215 mass spectrometer with faraday cup detector on line with glass extraction system. Samples progressively degassed in double-vacuum resistance furnace for 20 min in 10–12 steps ranging from 700 to 1550°C. Reactive gasses removed by SAES getters. Age calculations: weighted-mean ages weighted by fraction of potassium-derived ^{39}Ar released. Decay constant and isotopic abundances after Steiger and Jäeger (1977). Complete data set in "Electronic Supplements", Appendix A. 2. New Mexico Geochronology Research Laboratory: weighted-mean ages from single-crystal laser-fusion analyses. Sample irradiation: sanidine separates irradiated in machined Al discs for 7 h, D-3 position, Nuclear Science Center, College Station, TX. Neutron flux monitored by interlaboratory standard Fish Canyon Tuff sanidine FC-1 with an assigned age of 27.84 Ma (Deino and Potts, 1990), equivalent to Mmhb-1 at 520.4 Ma (Samson and Alexander, 1987). Instrumentation: Mass Analyzer Products 215-50 mass spectrometer on line with automated, all-metal extraction system at New Mexico Geochronology Research Laboratory, Socorro. Individual sanidine crystals (15 per sample) were fused in vacuo by a 10 W continuous CO_2 laser. Reactive gasses removed for 1–2 min by SAES GP-50 getters operated at 20°C and ~450°C. Age calculations: weighted-mean ages calculated by inverse variance weighting (Taylor, 1997). Decay constant and isotopic abundances after Steiger and Jäeger (1977). Complete data set in "Electronic Supplements", Appendix B. Analytical parameters: electron multiplier sensitivity $= 7 \times 10^{-17}$ moles/pA; average system blanks $= 260, 9.8, 2.1, 6.3, 7.7 \times 10^{-18}$ moles at masses 40, 39, 38, 37, 36, respectively. J-factors determined to a precision of ±0.2% by CO_2 laser-fusion of 4–6 single crystals from each of 4–6 radial positions around irradiation vessel. Correction factors for interfering nuclear reactions, determined using K-glass and CaF_2, $(^{40}Ar/^{39}Ar)_K = 0.00020 \pm 0.0003$; $(^{36}Ar/^{37}Ar)_{Ca} = 0.00026 \pm 0.00002$; and $(^{39}Ar/^{37}Ar)_{Ca} = 0.00070 \pm 0.00005$

	Sample	Location	Latitude	Longitude	Dip	Unit	Material	*n*	Age (Ma)	Source
A	JF-94-79	CH-AE	35°39′06″	115°00′49′	15°E	Tdb	gm	6	12.79 ± 0.22	1
B	JF-94-82	CH-AE	35°37′02″	114°59′57′	24°E	Tdt	sd	6	15.00 ± 0.03	1
C	JF-96-45	CH-AE	35°36′58″	114°59′58′	28°E	Tb	sd	15	15.21 ± 0.04	2
D	JF-94-80	CH-AE	35°37′40″	115°00′24′	30°E	Thb	gm	6	16.03 ± 0.07	1
E	JF-94-81	CH-AE	35°37′27″	115°00′32′	45°E	Thb	gm	4	16.50 ± 0.06	1
F	JF-94-70	CH-AW	35°34′05″	115°02′01′	44°W	Thb	gm	4	15.81 ± 0.05	1
G	JF-94-71	CH-AW	35°34′28″	115°01′34′	63°W	Thb	gm	5	16.01 ± 0.07	1
H	JF-96-41	SHR	35°34′12″	114°59′09′	35°W	Tdt	sd	15	14.98 ± 0.04	2
I	JF-96-42	SHR	35°34′17″	114°59′07′	45°W	Tb	sd	15	15.26 ± 0.04	2
J	JF-96-44	SHR	35°34′28″	114°58'53"	40°W	Tb	sd	15	15.22 ± 0.04	2
K	JF-94-64	SHR	35°32′39″	114°58′10′	45°W	Thb	gm	5	15.66 ± 0.08	1
L	JF-94-63	SHR	35°32′11″	114°58′09′	60°W	Thb	gm	3	15.98 ± 0.05	1
M	JF-94-62	SHR	35°31′43″	114°58′04′	75°W	Thr	bt	7	16.21 ± 0.17	1
N	JF-94-61	SHR	35°33′29″	114°57′49′	75°W	Thr	bt	5	16.26 ± 0.15	1
O	JF-94-78	CH-b	35°35′57″	115°04′15′	27°E	Tha	gm	7	18.27 ± 0.09	1

the McCullough Range fault. This is consistent with the interpretation that this fault merges southward with the breakaway to an east-dipping detachment system in the Whipple domain. Although not linked to breakaway faults, the west-dipping Keyhole Canyon and Copper Mountain faults within the southern part of the east-tilted Lake Mead domain may also have listric geometries. However, the geometry of these west-dipping faults is obscured by the late Tertiary–Quaternary alluvium in the southern part of the Eldorado basin.

Both listric and anti-listric (i.e. dip increases with depth) geometries are inferred for many faults within the Highland Range. Where tilts of hanging walls are less than that of footwalls, anti-listric geometries are interpreted. This is relatively common within and near the hinge zone of the anticline. Listric geometries are inferred in cases where hanging walls are tilted more steeply than footwalls, which is especially common near the hinge zone of the syncline (Fig. 5a). In much of the Highland Range, similar magnitudes of tilt characterize the hanging walls and footwalls of individual faults, suggesting a planar geometry. Slightly curved, concave-upward geometries (i.e. slightly listric) are inferred, however, for many of these faults (Fig. 5), because movement probably coincided with deposition of synextensional strata. In such cases, concave-upward geometries would result from the upward

Fig. 8. Generalized stratigraphic columns showing approximate tilts, relative unit thicknesses, and $^{40}Ar/^{39}Ar$ age spectra and ideograms for dated units in the southeastern and central Highland Range. Circled letters correspond to sample locations in Fig. 4. Although portrayed on the east-tilted stratigraphic column, samples F and G (shown with asterisks) were actually collected from the west-tilted domain on the west limb of the anticline (see Fig. 4). For age spectra: T_p, weighted mean plateau age; T_m, mean age not strictly satisfying plateau criteria; *n*, number of steps in age spectra used to calculate age. Patterns and labels are the same as in Fig. 4, with the exception of the following units: Tca, basal arkosic conglomerate; Tps, 18.5 Ma Peach Springs Tuff; Tb, tuff of Bridge Spring; Tdt, tuff of Mount Davis; Tdb, basalt lavas of the Mount Davis Volcanics; Tcb, megabreccia of basaltic trachyandesite lavas; Tbr, 15.0–15.2 Ma megabreccia and conglomerate.

propagation of individual faults at steep dips as deeper, older segments were progressively rotated to shallower dips through domino-like block tilting.

In the Highland Range, major gently dipping normal faults, such as the Highland fault, are found only in the steeply tilted southeastern part of the range. Such faults are cut by more steeply dipping normal faults (Fig. 5b). These relations suggest that the gently dipping normal faults originally developed at relatively steep dips and were rotated to their present shallow dips by domino-like block tilting (e.g. Proffett, 1977) of their respective footwalls and hanging walls. It is also noteworthy that fault-bedding intersection angles (as measured downward from bedding to the fault) commonly approach and, in many cases, exceed 90°. These relations imply that such faults either formed at relatively steep dips (>70°) or developed after significant tilting.

3.2. Stratigraphy and geochronology

The Miocene rocks in the Highland Range are deformed by both normal faults and folds. Determining the relative timing of folding and extension is critical for ascertaining the origin of the folds. Stratigraphic and $^{40}Ar/^{39}Ar$ geochronologic studies were conducted to correlate volcanic units, determine whether the limbs of the folds developed synchronously, and ascertain whether folding coincided with regional extension.

Early to middle Miocene volcanic rocks dominate the Highland Range. The Miocene section ranges up to 3.5 km in thickness and rests directly on Early Proterozoic gneiss and amphibolite. On the basis of differences in the Miocene stratigraphy, the Highland Range can be divided into two lithologic domains, which are separated in the south by the Highland Pass fault and in the north by the topographic and structural low of the syncline (Figs. 4 and 5). The central domain, mainly west of the Highland Pass fault, is characterized by a 2–3-km-thick lower sequence of mafic to intermediate lavas capped, along its margins, by two rhyolitic ash-flow tuffs, conglomerate, and isolated basalt lavas (Fig. 8). The stratigraphy of the southeastern domain is more complex and includes, in ascending order, a 1.5-km-thick sequence of intermediate lavas, 1-km-thick section of rhyolite lavas and tuffs, a relatively thin (up to 350 m) sequence of mafic lavas, two rhyolitic ash-flow tuffs, and capping middle to late Miocene conglomerate and megabreccia. The mafic and felsic volcanic rocks in the southeastern Highland Range and the lower sequence of mafic to intermediate lavas in the central Highland Range are informally referred to as the volcanics of the Highland Range, because they appear to be derived from sources either within or proximal to the Highland Range.

3.2.1. $^{40}Ar/^{39}Ar$ geochronology: methods and results

$^{40}Ar/^{39}Ar$ studies were conducted in the central and southeastern Highland Range to facilitate correlations of volcanic stratigraphy and help constrain the relative timing of folding and extension. A total of 15 samples were collected and analyzed. These include eight samples of mafic to intermediate lavas, two rhyolitic lavas, and five samples of rhyolitic tuff (Fig. 8; Table 1).

Sanidine or biotite separates were prepared from the rhyolites using standard density, magnetic, and hand-picking techniques. Concentrates of the fine-grained potassium-bearing groundmass from trachyandesite and basalt samples were prepared by removing olivine, pyroxene, and plagioclase phenocrysts. $^{40}Ar/^{39}Ar$ analyses were carried out at the Branch of Isotope Geology at the U.S. Geological Survey in Denver using resistance-furnace, incremental-heating techniques, and at the New Mexico Geochronology Research Laboratory using single-crystal CO_2 laser-fusion methods. Sample irradiation and analytical procedures and parameters are provided in the notes of Table 1.

$^{40}Ar/^{39}Ar$ results are summarized in Table 1 and Fig. 8, and are further detailed in "Electronic Supplements" on the journal's homepage: http://www.elsevier.com/locate/jstrugeo, Appendices A and B. Age spectra from incrementally heated groundmass concentrates and biotite and sanidine separates are relatively flat except for discordance of some initial, low-temperature steps (Fig. 8). For the step-heated samples, the criteria of Fleck et al. (1977) were used to establish whether the results of an individual age spectrum constituted a plateau date. For the purposes of this study, a plateau requires that two or more contiguous gas fractions yield apparent ages that are statistically identical, using the critical value test of Dalrymple and Lanphere (1969), and together constitute greater than 50% of the total potassium-derived ^{39}Ar released during the step-heating experiment. Weighted-mean plateau ages were calculated for the five age spectra that satisfied this criteria (Fig. 8). For the remaining six step-heated samples, weighted mean ages were calculated for the flattest parts of age spectra, which approached but did not completely satisfy the rigid plateau criteria described above (Fig. 8; "Electronic Supplements", Appendix A). Although not satisfying the plateau criteria, we consider these apparent ages to be reasonable estimates of geologic age. Weighted-mean ages of step-heated samples range from 18.27 ± 0.09 to 12.79 ± 0.22 Ma, and analytical uncertainties range from ± 0.2 to $\pm 1.7\%$ (all errors reported for mean ages herein are at $\pm 2\sigma$).

Ages of individual crystals from each of the four sanidine separates analyzed by laser fusion form simple Gaussian distributions (Fig. 8), with MSWD values (mean square of weighted deviates; "Electronic Supplements", Appendix B) ranging from 0.62 to 1.47, well within the 95% confidence interval for single populations suggested by Mahon (1996). Weighted-mean ages for these samples range from 14.98 ± 0.04 to 15.26 ± 0.04 Ma, and analytical uncertainties are near $\pm 0.25\%$.

3.2.2. Regional ash flows

The 15.2 Ma tuff of Bridge Spring and 15.0 Ma tuff of

Fig. 9. Tuff of Bridge Spring (Tb) pinchout looking northeast on the east limb of the anticline. $^{40}Ar/^{39}Ar$ samples B and C were collected here (see northeast part of map area, Fig. 4). In this area, the 15.0 Ma tuff of Mount Davis (Tdt) directly overlies either the 15.2 Ma tuff of Bridge Spring, with only a thin paleosol between the two, or basaltic trachyandesite lavas in the volcanics of the Highland Range (Thb), which have yielded $^{40}Ar/^{39}Ar$ dates ranging from 16.0 to 16.5 Ma about 1 km to the northwest.

Mount Davis are two distinct, regionally extensive ash-flow tuffs that originally blanketed much of the Highland Range and surrounding region. The tuff of Bridge Spring was first described by Anderson (1971) in the northern Eldorado Mountains. It extends from the southern White Hills on the east (Price and Faulds, 1999) to the McCullough Range on the west (Morikawa, 1994) and from the northernmost Eldorado Mountains (Anderson, 1971; Gans et al., 1994) southward to the southern Black Mountains. The tuff of Mount Davis was first described by Faulds (1995) in the Lake Mohave area and may not be as widespread as the tuff of Bridge Spring. Its known distribution stretches from the central Black Mountains westward to the Highland Range and between the latitudes of Nelson and Searchlight, Nevada (Fig. 3). Although multiple cooling units were noted in the tuff of Bridge Spring, previous studies failed to recognize the tuff of Mount Davis in the Highland Range (Bingler and Bonham, 1973; Davis, 1984; Morikawa, 1994; Olson, 1996). This is not surprising, however, because the tuff of Mount Davis commonly rests directly on (Fig. 9), and is compositionally similar to, the tuff of Bridge Spring. Thus, it can be easily mistaken for an upper cooling unit within the tuff of Bridge Spring. The tuff of Mount Davis may therefore be more widespread than presently thought.

The two tuffs can, however, be distinguished by subtle differences in phenocryst assemblages, paleomagnetic reference directions, and in some areas by intervening sequences of conglomerate, megabreccia, and/or mafic lavas. In the southeastern Highland Range, for example, a thin (typically less than 20 m thick) sequence of megabreccia, of presumed rock-avalanche origin (cf. Yarnold and Lombard, 1989), and conglomerate commonly separates the tuffs of Mount Davis and Bridge Spring (Fig. 8). Although both tuffs have reverse magnetic polarity, the declination of their respective paleomagnetic reference directions differs by about 20° and is statistically significant at the 95% confidence interval (Faulds and Olson, 1997). In contrast to the tuff of Mount Davis, the tuff of Bridge Spring has ubiquitous sphene (sphene is rare in the tuff of Mount Davis), generally fewer phenocrysts, less abundant biotite and plagioclase, and typically finer-grained sanidine (Faulds and Bell, 1999).

In addition, the $^{40}Ar/^{39}Ar$ results permit unambiguous identification of the tuffs of Bridge Spring and Mount Davis (Figs. 8 and 10). An age-probability distribution diagram combining incremental-heating and laser-fusion data (Fig. 10) demonstrates the clear distinction between the 15.0 Ma tuff of Mount Davis and the 15.2 Ma tuff of Bridge Spring.

The tuff of Bridge Spring may have been derived from a caldera in the northern part of the Eldorado basin (Gans et al., 1994). The source of the tuff of Mount Davis is unknown, but similarities in age, composition, and distribution suggest that both tuffs were erupted from the same cauldron. In any case, both tuffs are important time-stratigraphic and structural markers in the northern Colorado River extensional corridor and nicely chronicle increments of Tertiary extension.

3.2.3. Central Highland Range

In ascending order, the Miocene section in the central part of the Highland Range consists of: (1) a 2–3-km-thick section of early to middle Miocene (18.3–16.0 Ma) basaltic

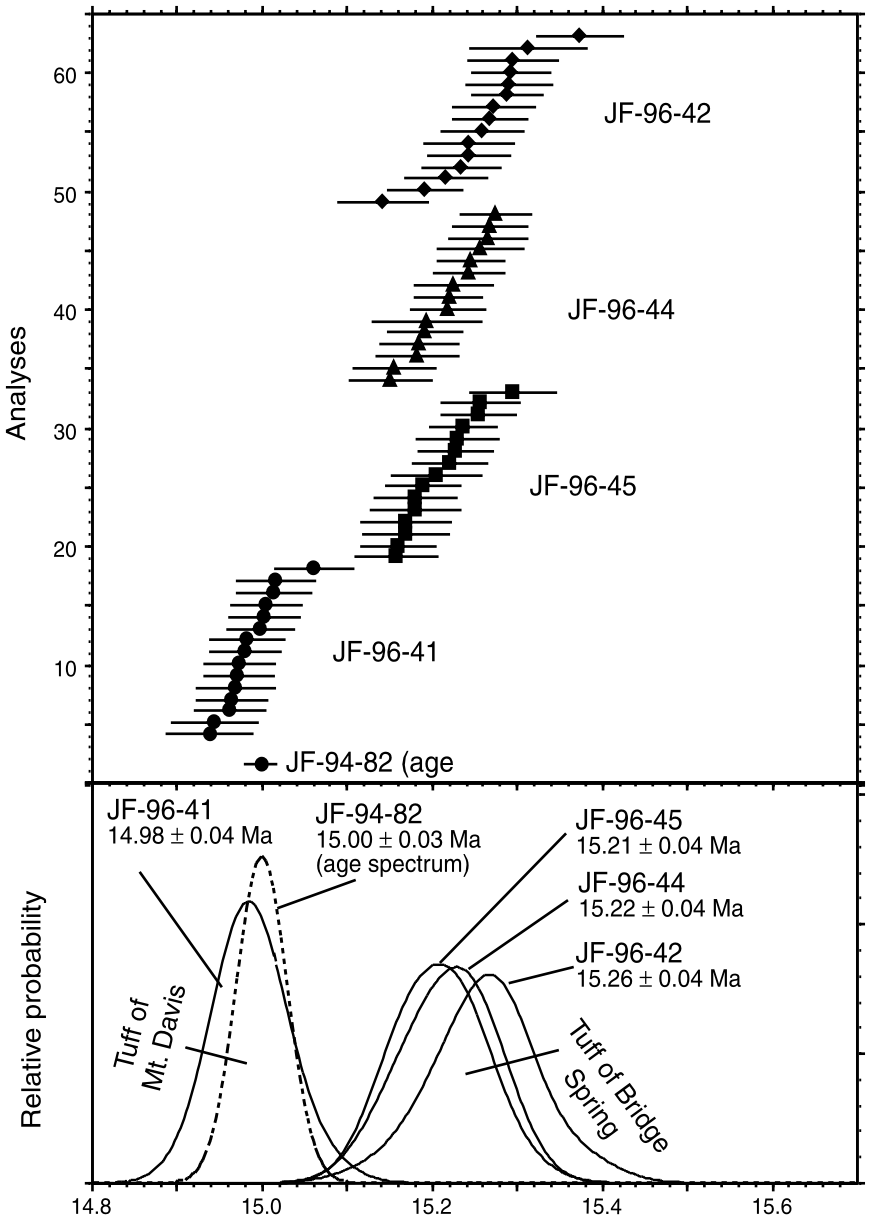

Fig. 10. Age-probability distribution diagram (ideogram) combining incremental-heating and laser-fusion data from sanidine separates of the 15.0 Ma tuff of Mount Davis and the 15.2 Ma tuff of Bridge Spring. The age-probability distribution curve is calculated by the method of Deino and Potts (1992).

trachyandesite and trachyandesite lavas and associated volcanic breccias and lahars (Davis, 1984; Feuerbach et al., 1999), which are grouped with the volcanics of the Highland Range and nonconformably overlie Early Proterozoic gneiss and amphibolite; (2) as much as about 1 km of conglomerate containing clasts of both early Miocene volcanic rocks and Proterozoic gneiss (Davis, 1984); (3) the 15.2 Ma tuff of Bridge Spring; (4) the 15.0 Ma tuff of Mount Davis; and (5) as much as approximately 300 m of middle to late Miocene conglomerate that includes intercalated 12.8 Ma basalt flows in the northeast (Figs. 4 and 8; Table 2).

The 18.3–16.0 Ma age and basaltic trachyandesite to trachyandesite composition suggest a correlation of the volcanics of the Highland Range with the 18.7–15.5 Ma (Darvall, 1991) lower Patsy Mine Volcanics of Anderson et al. (1972) in the northern Eldorado Mountains (Fig. 3; Table 2). Mafic to intermediate lavas in the volcanics of the Highland Range thicken northward, suggesting a possible volcanic center in the northern part of the range (mainly north of the area shown in Fig. 4) (Davis, 1984).

The overlying middle Miocene conglomerate pinches out toward the hinge zone of the anticline but thickens to the southwest (Figs. 4 and 5a). This southwestward thickening wedge and abundant clasts of Proterozoic rock suggest a fanglomerate origin for the conglomerate, with a provenance in the uplifted crystalline terrane of the southern McCullough Range, which must have been exposed ~16–15.2 Ma.

Table 2
Tertiary stratigraphy of the Highland Range, Southern Nevada. Symbol designations are the same as in Figs. 4 and 8. For locations correlatives and references: CREC, Colorado River extensional corridor; HRC, central Highland Range; HRS, southern Highland Range; ML, Lake Mohave area; NCREC, northern Colorado River extensional corridor; NN, northern Newberry Mountains; other abbreviations are the same as in Fig. 3

Stratigraphic unit	Symbol	Composition	Location	Age	Correlatives	References
Unnamed	Tc, Tcb	Conglomerate, sandstone, megabreccia	HRS, HRC	15.0– ~ 11 Ma	Sedimentary units in Mt. Davis Volcanics-SE, ML, CB	SE, ML, CB-(Faulds, 1995; 1996)
Mt. Davis Volcanics	Tdb	Basalt lavas	HRC, SE, NE, CB,	12.8 Ma	Mt. Davis Volcanics-NE, NB, SE, CB	NE, NB- Anderson (1977, 1978); Anderson et al. (1972); SE, CB- Faulds (1995, 1996)
Tuff of Mt. Davis	Tdt	Rhyolite tuff	HRC, HRS, SE, CB	15.0 Ma	Tuff of Mt. Davis-ML, CB	HRS- Faulds and Bell (1999); CB, ML- Faulds (1995, 1996); Faulds and Olson (1997)
Megabreccia	Tbr	Megabreccia	HRC, HRS	15.2–15.0 Ma		HRS- Faulds and Bell (1999)
Tuff of Bridge Spring	Tb	Rhyolite tuff	HRC, HRS, NE, SE, CB, SWH, SB, MR	15.2	Tuff of Bridge Spring-NE, NB, MR, SE, ML, CB; Tuff of Red Willow Spring-SWH	NE, NE- Anderson et al. (1972); Darvall (1991); Gans et al. (1994); MR- Morikawa (1994); SE, ML, CB- Faulds (1995, 1996); Faulds et al. (1995); SWH- Price and Faulds (1999); HRS- Faulds and Bell (1999)
Unnamed	Tsb	Megabreccia, conglomerate, sandstone	HRS, HRC	16.0–15.2 Ma	Sedimentary units in Mt. Davis Volcanics-SE, ML, CB	SE, ML, CB- Faulds (1995)
Volcanics of the Highland Range	Thr	Rhyolite lavas, tuffaceous rocks	HRS, NN	16.3–16.0 Ma	Unnamed rhyolite lavas-NN; lowermost volcanics of Red Gap Mine-CB	HRS- Olson (1996); Faulds and Bell (1999); NN- Ruppert (1999); CB- Faulds et al. (1995)
	Thb	Basaltic trachyandesite lavas	HRC, HRS	18.3–15.2 Ma	Lower Patsy Mine Volcanics-HRC, NE; volcanics of Fire Mt.-CB, ML	HRC- Davis (1984); HRS- Olson (1996); Faulds and Bell (1999); NE- Anderson et al. (1972); Darvall (1991); CB, ML- Faulds (1996)
Volcanics of Dixie Queen Mine	Tq	Trachydacite-trachyandesite lavas	HRS, SE, SB, NN	18.5–16.3 Ma	Volcanics of Dixie Queen Mine-CB, NN; lower Patsy Mine Volcanics-NE, NB	HRS- Faulds and Bell (1999); CB- Faulds et al. (1995); NN- Ruppert (1999); NE, NB- Anderson et al. (1972); Darvall (1991); Anderson (1977, 1978)
Peach Springs Tuff	Tps	Rhyolite tuff	HRS, SE, NE, CB, SB, NB	18.5 Ma	Peach Springs Tuff-CP, CREC, NN, ML	CREC, CP- Glazner et al. (1986); Nielson et al. (1990); NN- Ruppert (1999); ML- Faulds (1995)
Unnamed	Tca	Arkosic conglomerate	NCREC	~ 20–18.5 Ma	Conglomerate of Cottonwood Pass-CB, ML	CB, ML- Faulds (1995)
Searchlight pluton	Tsl	Granitic pluton	SE	16.5 Ma		SE- Bachl (1997)
Unnamed	Xg	Early Proterozoic gneiss	HRS, SE, SMR	~ 1.6–1.8 Ga		HRS, SE- Faulds and Bell (1999)

The tuffs of Bridge Spring and Mount Davis and overlying conglomerate and basalt lavas crop out on the limbs of the anticline but are missing from the hinge zone, except on the southeast end of the southward plunging anticline near the Highland Pass fault (Fig. 4). On the east limb of the anticline, the tuff of Bridge Spring thins and pinches out westward toward the hinge zone (Fig. 9). Both tuffs thin and pinch out northward on the west limb. Thus, the hinge zone of the anticline appears to have been a topographic high that restricted deposition and/or induced erosion of units 16.0–12.8 Ma, with less deposition and/or more erosion near the northwest end of the anticline, where the upper conglomerate locally rests on Proterozoic gneiss in the core of the fold (Fig. 4).

The upper middle to late Miocene conglomerate and intercalated 12.8 Ma basalt flows correlate with the Mount Davis Volcanics, a widespread synextensional unit of mafic lavas and associated clastic rocks in the northern part of the corridor (Anderson et al., 1972; Faulds, 1995, 1996). Clasts of Proterozoic gneiss are common within this conglomerate and record significant erosion of the southern McCullough Range between 15.0 and 12.8 Ma. Thus, beginning 15.7–16.0 Ma and continuing to at least 12.8 Ma, fanglomerates were apparently shed from the southern McCullough Range into developing basins to either side of the anticlinal hinge (Fig. 4).

3.2.4. Southeastern Highland Range

The volcanic stratigraphy of the southeastern Highland Range is more felsic than that in the central part of the range. In ascending order, the stratigraphy in the southeast includes: (1) a thin (<60 m) poorly exposed, basal sequence of arkosic conglomerate and the 18.5 Ma Peach Springs Tuff (cf. Glazner et al., 1986; Nielson et al., 1990), which nonconformably overlie Early Proterozoic gneiss and crop out only in the southeasternmost part of the area (Fig. 4); (2) a 1.5-km-thick sequence of approximately 18.5–16.3 Ma trachydacite and trachyandesite lavas, which rest conformably on the Peach Springs Tuff and basal conglomerate; (3) as much as 1 km of 16.3–16.0 Ma rhyolite flows and tuffaceous strata; (4) up to 350 m of 16.0–15.2 Ma basaltic trachyandesite flows; (5) 16.0–15.2 Ma megabreccia (of probable rock avalanche origin), volcaniclastic conglomerate, and sandstone that locally exceeds 200 m in thickness; (5) up to 300 m of the 15.2 Ma tuff of Bridge Spring and 15.0 Ma tuff of Mount Davis, locally separated by thin (typically <20 m) rock avalanche deposits and conglomerate; and (6) as much as 500 m of middle to late Miocene conglomerate, sandstone, and rock avalanche deposits (Figs. 4, 5, and 8; Table 2). The granitic Searchlight pluton (Bachl, 1997) invades the lower sequence of intermediate lavas in the southeasternmost part of the area (Fig. 4).

The lower 18.5–16.3 Ma trachydacite and trachyandesite lavas correlate with the volcanics of Dixie Queen Mine in the central Black Mountains (Faulds et al., 1995), as evidenced by similar compositions and nearly identical ages. The 16.3–16.0 Ma felsic volcanic sequence rests conformably on the volcanics of Dixie Queen Mine. Its lower part consists primarily of rhyolite lava, whereas the upper portion is dominated by nonwelded tuffs and tuffaceous sedimentary rocks. The overlying sequence of 16.0–15.2 Ma basaltic trachyandesite lavas thins from about 350 to 35 m southward across the southeastern Highland Range. Both the felsic volcanic sequence and overlying basaltic trachyandesite lavas are grouped with the volcanics of the Highland Range. The felsic sequence pinches out northwestward near the boundary between the central and southeastern parts of the Highland Range, where it interfingers with and gives way to the thick pile of basaltic trachyandesite lavas in the central Highland Range (Figs. 4 and 5). As noted previously, basaltic trachyandesite members in the volcanics of the Highland Range continue to thicken northward toward a possible source in the northern Highland Range.

Rock avalanche deposits and/or a relatively thin (<80 m) sequence of conglomerate locally overlie the 16.0–15.2 Ma basaltic andesite lavas. The rock avalanche deposits include megabreccia of Proterozoic gneiss, early Miocene trachydacite, and early to middle Miocene basaltic trachyandesite. Proterozoic detritus is also common in the conglomerate. In the west near the Highland Pass fault, the clasts and megabreccia of gneiss resemble exposed basement in the southern McCullough Range, whereas to the east near the Searchlight fault (Fig. 4) such detritus more closely matches basement rock types exposed in the southern Eldorado Mountains. These relations indicate significant basin development in the southeast Highland Range and uplift of surrounding crystalline terranes between 15.7 and 15.2 Ma.

The 15.2 Ma tuff of Bridge Spring crops out across the entire southeastern Highland Range. It rests directly on either the volcanics of the Highland Range or the megabreccia–conglomerate sequence. It thickens westward in the west-tilted half graben in the hanging wall of the Highland Pass fault and toward the hinge zone of the syncline. As noted previously, however, it thins dramatically westward and pinches out on the west limb of the syncline toward the hinge zone of the anticline. In contrast to that in the central Highland Range, thin sequences (typically <20 m thick) of rock avalanche deposits or bouldery, matrix-supported conglomerate, of probable debris flow origin, are common between the tuff of Bridge Spring and tuff of Mount Davis in the southeast. Similar to the tuff of Bridge Spring, the tuff of Mount Davis also thickens westward within both the west-tilted hanging wall of the Highland Pass fault and toward the synclinal hinge zone (Fig. 4). In the southernmost part of the range, the tuff of Mount Davis is absent, but this may be a consequence of erosion, as Miocene sections younger than 15.2 Ma are missing.

The capping sequence of middle to late Miocene

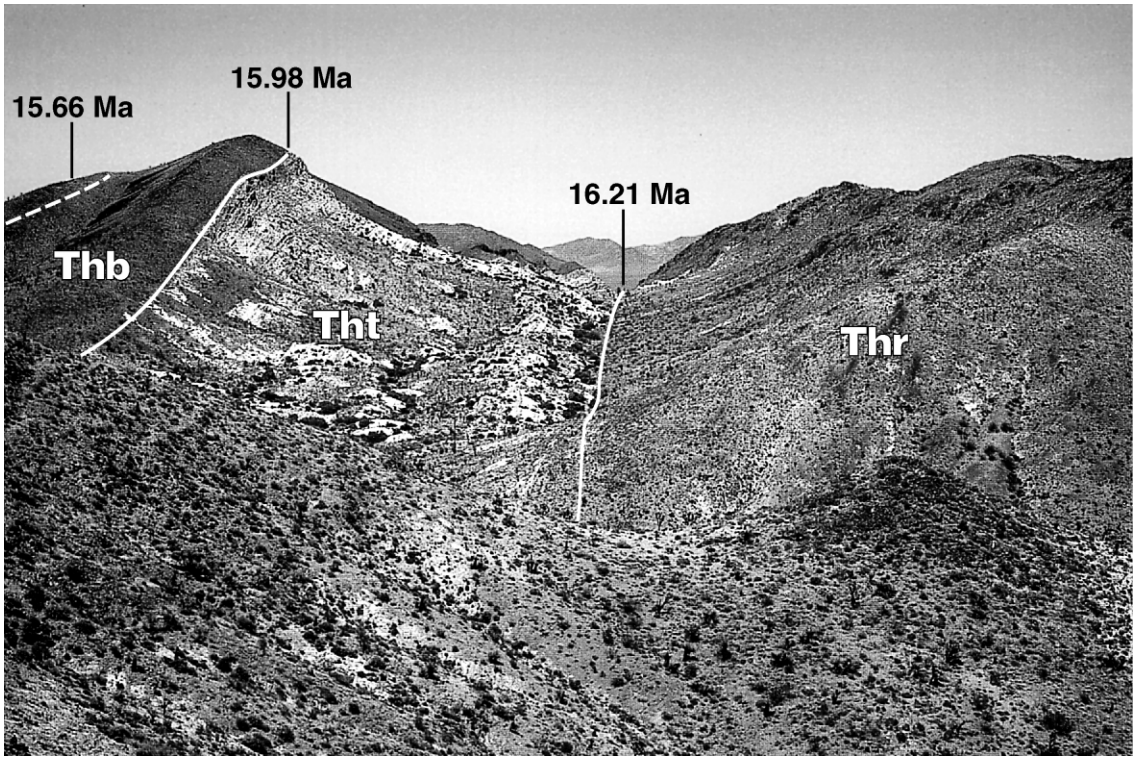

Fig. 11. Tilt fanning in the southeastern Highland Range looking north. West dips progressively decrease up-section in this area from about 75° in 16.21–16.26 Ma rhyolite lavas (Thr), to 60° in 15.98 Ma basaltic trachyandesite lavas (Thb), and to approximately 45° in 15.66 Ma basaltic trachyandesite lavas. $^{40}Ar/^{39}Ar$ samples K, L, M, and N were collected from this area (see Fig. 4; Table 1).

conglomerate, sandstone, and megabreccia conformably overlies the tuff of Mount Davis and has the same general distribution as the tuffs of Mount Davis and Bridge Spring. These sedimentary rocks are thickest (~500 m) near the east-dipping Highland Pass fault (Figs. 4 and 5). Clasts of Early Proterozoic gneiss are common in the conglomerate and increase in abundance and size to the west, suggesting a primary source in the crystalline terrane of the southern McCullough Range. The conglomerate in the southeast part of the range correlates with the capping middle to late Miocene conglomerate on the west limb of the anticline in the hanging wall of the McCullough Range fault and represents the more distal part of the fanglomerate sheet shed from the southern McCullough Range (Figs. 4 and 5). However, megabreccia intercalated within the conglomerate is generally composed of basaltic trachyandesite

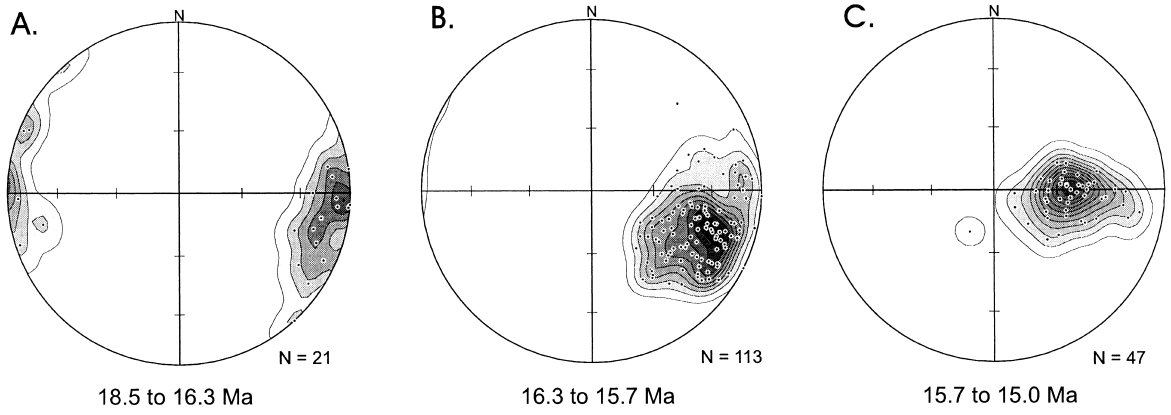

Fig. 12. Lower-hemisphere equal-area stereographic projections of poles to layering and bedding in Miocene rocks of the southeastern Highland Range showing a progressive, up-section decrease in dip. These density contour plots indicate the percent of data per 1% area. *N*, number of measurements (shown as dots). (A) 18.5–16.3 Ma volcanics of Dixie Queen Mine. Mean orientation of layering and bedding is N3°E, 85°NW. Contour intervals are at 0, 2, 4, 6, 8, and 10% per 1% area. (B) 16.3–15.7 Ma strata (mainly volcanics of the Highland Range). Mean orientation is N16°E, 63°NW. Contour intervals are at 0, 2, 4, 6, 8, 10, 12, 14, and 16% per 1% area. (C) 15.7 to 15.0 Ma strata (mainly tuffs of Bridge Spring and Mount Davis). Mean orientation is 0°, 38°W. Contour intervals are at 0, 2, 4, 6, 8, 10, 12, 14, 16, 18, 20, and 22% per 1% area.

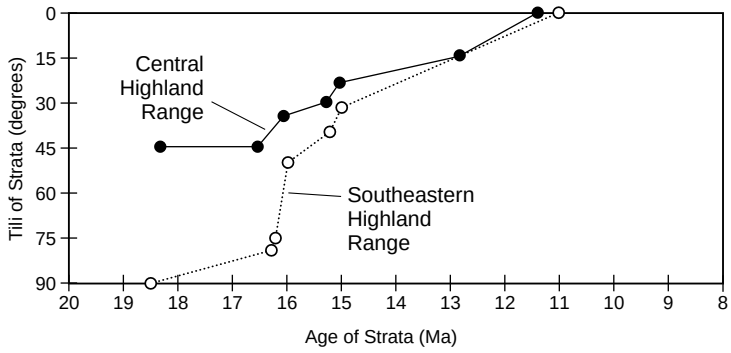

Fig. 13. Tilt versus age plots for volcanic stratigraphy of the Highland Range utilizing the new $^{40}Ar/^{39}Ar$ dates and average tilts of strata shown in Table 1 (see also Fig. 8). Steeper sloping lines correspond to faster rates of tilting and, by implication, greater rates of extension. In the central Highland Range, tilting rates locally peaked at ~80°/m.y. between ~16.0 and 15.8 Ma on the west limb of the anticline (not shown here) but generally averaged 20–30°/m.y. between ~16.2 and 15.0 Ma. In the southeastern Highland Range, tilting rates peaked at ~75°/Ma between ~16.2 and 16.0 Ma and ranged from 25 to 50°/m.y. between 16.0 and 15.0 Ma. Tilting rates throughout the central Highland Range slowed to less than 10–25°/m.y. between 15.8 and 12.8 Ma.

lava derived from nearby exposures in the footwall of the Highland Pass fault.

4. Timing of deformation

The style and timing of deformation are most easily addressed in the southeastern Highland Range, which lies fully within the west-tilted Whipple domain and corresponds to the upper part of the large aforementioned west-tilted fault block. This area is riddled by gently to steeply dipping normal faults and characterized by significant tilt fanning (Fig. 11), whereby the magnitude of tilting progressively decreases up-section (Fig. 5b, see west part of cross-section). The tilting in this area is clearly a manifestation of extensional strain and can therefore be used to constrain the timing of regional extension. The onset of tilting was determined by dating the youngest, most steeply tilted unit, above which significant tilt fanning begins. An upper limit of extension was constrained by dating the youngest, most gently tilted strata and by regional relations.

In the southeastern Highland Range, dips are essentially conformable in the lower sequence of trachydacite and trachyandesite lavas (volcanics of Dixie Queen Mine) but progressively decrease up-section from about 85° in the lowermost part of the overlying rhyolite unit to less than 15° in the capping conglomerate (Fig. 5). West dips average 85° in the 18.5–16.3 Ma volcanics of Dixie Queen Mine, 63° in the 16.3–15.7 Ma rhyolites and basaltic trachyandesites of the Highland Range volcanics, and 38° in the 15.2–15.0 Ma tuffs of Bridge Spring and Mount Davis (Figs. 11 and 12). The upper conglomerate rests conformably on the tuff of Mount Davis but is tilted less up-section, with dips of 15–20° in the younger part of the sequence. The youngest, most steeply dipping unit, found near the base of the Highland Range volcanics, yielded an $^{40}Ar/^{39}Ar$ age on biotite of 16.21 ± 0.17 Ma (Fig. 8m; Table 1), which signifies the approximate onset of tilting and extension. Tilting rates peaked at approximately 75°/m.y. between 16.2 and 16.0 Ma (Fig. 13). About 50% of the tilting in the southeast Highland Range occurred between 16.2 and 15.0 Ma, prior to deposition of the tuff of Mount Davis.

In the central Highland Range, dips are essentially conformable in the lower 2 km of the Miocene section but, beginning in the upper part of the volcanics of the Highland Range, progressively decrease upward on both limbs of the anticline. The youngest most steeply dipping unit was dated at 16.01 ± 0.07 Ma (Fig. 8g) on the west limb and 16.50 ± 0.06 Ma (Fig. 8e) on the east limb. The latter date is interpreted to be a maximum age due to the lack of a well defined plateau in the age spectrum. On the west limb, dips decrease up-section from 63 to 44° in the 16.1–15.8 Ma upper part of the Highland Range volcanics, to about 30° in the 15.0 Ma tuff of Mount Davis, and to about 15° in capping conglomerate. On the east limb, dips decrease up-section from 45 to 30° in the 16.5–16.0 Ma upper part of the Highland Range volcanics, to 24° in the tuff of Mount Davis, and to 15° in the 12.8 Ma basalt lavas (Fig. 8; Table 1).

Thus, on both the east and west limbs of the anticline, tilting began approximately 16.5–16.1 Ma, and about 50% of the tilting had occurred by 15.0 Ma. This coincides with the timing of tilting and extension in the southeastern Highland Range. Rates of tilting in the central Highland Range averaged 20–30°/m.y. between about 16.2 and 15.0 Ma (Fig. 13). This is much less than that to the southeast, as is the overall magnitude of tilting in the central Highland Range (Fig. 5).

The onset of extension in the southeastern Highland Range is slightly older than that documented in the central Black Mountains to the east (15.6–15.8 Ma; Faulds et al., 1995) and northern Eldorado Mountains to the northeast (about 15.5 Ma; Darvall, 1991), but is similar to that described in the northern Newberry Mountains to the southeast (about 16.2 Ma; Ruppert, 1999; Ruppert et al., 1999) (Fig. 3). It is also noteworthy that the onset and fastest

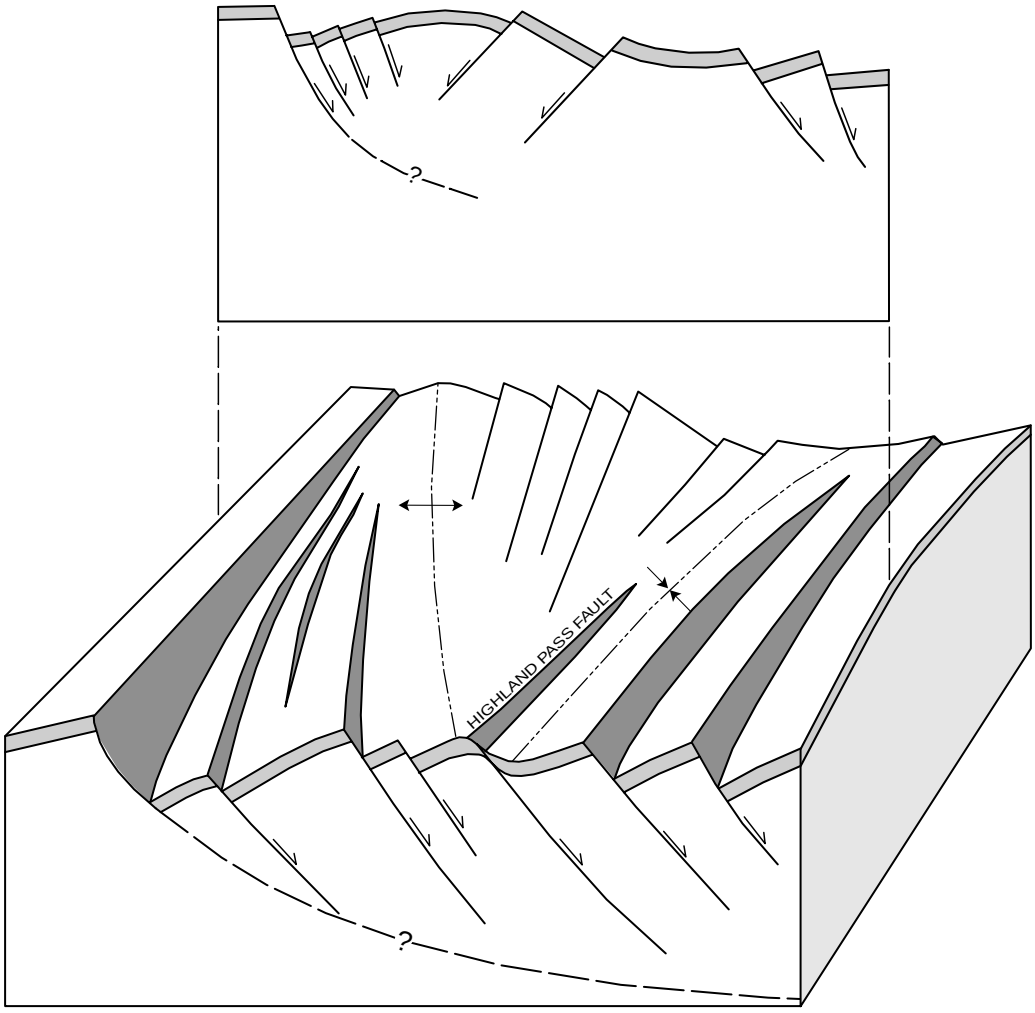

Fig. 14. Schematic three-dimensional block diagram of the central and southeastern Highland Range, showing the extensional anticline and syncline. The geometry of the folds was controlled by the relative dip directions, magnitude of offset, spacing, and amount of along-strike overlap of the oppositely dipping normal-faults. Movement on overlapping inwardly dipping faults generated the anticline, whereas overlapping outwardly dipping fault systems produced the syncline. It is noteworthy that the southern end of the syncline corresponds to a hanging wall syncline produced by normal drag along the northern tip of the east-dipping Highland Pass fault. Note also that the anticline consistently stands topographically higher than the syncline. The syncline becomes more symmetric to the north as the Highland Pass fault and associated drag- or fault-propagation fold terminate.

rate of tilting in the Highland Range immediately followed emplacement of the 10 + -km-thick, 16.5 Ma Searchlight pluton (Faulds et al., 1998).

The younger age limit for tilting and extension in the Highland Range is less well defined. The youngest, most gently tilted (~15°), dateable unit yet observed is the 12.79 ± 0.22 Ma basalt lava in the northeast part of the range (Fig. 8a). Similarly tilted basalt flows in the Lake Mohave area (Fig. 3) have also yielded 12.8–13.0 Ma $^{40}Ar/^{39}Ar$ ages (Faulds et al., 1995). Flat-lying to very gently dipping (<5°) strata in the Lake Mohave area directly to the east have consistently yielded ages of 11.3–11.6 Ma (Faulds et al., 1995; Faulds, 1996). These relations suggest that extension in the Highland Range was waning significantly by 12.8 Ma and had ceased by about 11 Ma.

5. Discussion

5.1. Origin of folds

Several features indicate that the anticline and syncline within the Highland Range are products of extensional strain. The limbs of the folds are parts of discrete half grabens and tilted fault blocks bounded by normal faults. For example, the west and east limbs of the anticline are half grabens in the hanging wall of the McCullough Range fault and Keyhole Canyon–Copper Mountain fault system, respectively. Similarly, the west-tilted eastern limb of the syncline is a half graben in the hanging wall of the Highland Pass fault (Figs. 4 and 5). Dips progressively decrease up-section in the half grabens indicating synextensional deposition of middle Miocene sedimentary and volcanic

rocks. $^{40}Ar/^{39}Ar$ dates of variably tilted units within the east- and west-tilted growth-fault basins in the Highland Range demonstrate that the opposing limbs of the folds developed synchronously during the middle Miocene (~16.5–11 Ma). The folding is coeval with extension in both the southeast Highland Range and nearby parts of the Colorado River extensional corridor (e.g. Anderson et al., 1972; Spencer, 1985; Faulds et al., 1995; Ruppert et al., 1999). Furthermore, normal faults dominate the entire range, and no major reverse faults were observed. Thus, several of the criteria established by Janecke et al. (1998) to distinguish extensional from contractional folds are satisfied in the Highland Range, including (1) near absence of reverse faults of the same age as the folds, (2) close spatial and temporal association of folds and normal faults, and (3) growth strata on the fold limbs.

Davis (1984) interpreted the anticline as a middle Miocene, northwest-trending flexure of brittle upper crust above an isostatically rebounding ramp within a major gently west-dipping detachment fault. The isostatically rebounding ramp model is not compatible, however, with the concomitant lateral truncation of both the anticline and regionally extensive conjugate normal faults and fault systems. Moreover, four large en échelon anticlines have now been documented in the Black Mountains accommodation zone, where the oppositely dipping normal-fault systems of the Whipple and Lake Mead domains overlap along strike (Faulds, 1994; Faulds and Varga, 1998). It is unlikely that each of these anticlines is associated with isostatically rebounding ramps in subjacent detachment faults. It is important to note, however, that at the time of Davis' study, accommodation zones were not recognized as inherent features in continental rifts nor was the Black Mountains accommodation zone identified.

The folds within the Highland Range developed within the belt of overlapping, oppositely dipping normal-faults that constitutes the Black Mountains accommodation zone. The geochronologic data indicate that the opposing normal-fault systems in the Highland Range were active contemporaneously and can therefore be considered conjugate sets.

Fault-bend folding was primarily responsible for producing the folds within the Highland Range. The anticline can be attributed to the intersection of opposing rollovers developed in the hanging walls of oppositely dipping normal faults that dip toward one another and overlap along strike (mainly the McCullough Range and Keyhole Canyon faults). The syncline formed where the overlapping, oppositely dipping fault systems dip away from one another (Figs. 5 and 14). Both listric and anti-listric normal faults partially accommodated the folding by inducing both differential tilting of adjacent fault blocks and bending strains within individual fault blocks.

A three-dimensional perspective of the Highland Range (Fig. 14) suggests, however, that other processes also played important, but subsidiary, roles in the folding. For example, the anomalous steep dips of east-tilted strata near the juncture of the anticline and syncline (e.g. east-tilted western limb of the syncline; Figs. 4 and 5a) were probably produced by fault-drag folding resulting from normal drag along the Highland Pass fault and/or development and subsequent breaching of a fault-propagation fold (e.g. Suppe, 1985) near the tip of the Highland Pass fault. The asymmetric southern part of the syncline merges northward with the more regional, symmetric syncline that originated largely through fault-bend folding (Fig. 14). In addition, displacement-gradient folding (e.g. Schlische, 1995; Janecke et al., 1998) influenced the geometry of the fault-bend fold that forms the west limb of the anticline, as evidenced by the spatial correspondence between the belt of anomalous, northwest-striking strata and a severe displacement gradient on the McCullough Range fault. Several features indicate that displacement on the McCullough Range fault decreases significantly northward near the northern tip of the anticline and northern terminus of the west-tilted domain. They include the northward narrowing and termination of the Piute basin (Fig. 3), little if any throw separating the northern Highland Range from the central part of the McCullough Range, and lack of Miocene strata in the southern McCullough Range. In the latter case, southward increasing offset on the McCullough Range fault presumably induced a southward increase in uplift of the footwall, which complemented the southward increase in subsidence of the Piute basin in the hanging wall. This led to either erosion or non-deposition of Miocene strata in the southern McCullough Range. The anomalous northwest strikes on the west limb of the anticline reflect the north limb of a transversely oriented, displacement gradient fold. Thus, multiple processes apparently produced the folds in the Highland Range. Multiple processes also generated extensional folds in the Rocky Mountain Basin and Range province (Janecke et al., 1998).

The oblique trends of the Highland Range anticline and syncline (relative to the strikes of major normal faults) reflect partial overlap between the opposing normal-fault systems (Fig. 1a and b). Each end of the anticline corresponds to an area in which one of the competing fault sets has minimal displacement. For example, both the west-dipping McCullough Range and east-dipping Keyhole Canyon faults lose displacement rapidly near the northwest and southeast ends of the anticline, respectively (Fig. 3). The rollover in the hanging wall of each fault does not end, however, at the fault tips but instead dies out where displacement on the related faults falls below some critical threshold (~1 km). Thus, the anticline does not actually connect the tips of individual, oppositely dipping normal faults. Conversely, the distance between the hinge of the rollover and mapped trace of the fault generally increases with the magnitude of fault displacement. However, several other factors also affect this relationship, including the curvature of the fault, depth to detachment, and folding mechanisms within the rollover (e.g. Dula, 1991).

Nevertheless, in cases where overlap between the oppositely dipping normal-fault systems is complete, as in the easternmost anticline of the Black Mountains accommodation zone (Varga et al., 1996; Faulds and Varga, 1998), the fold hinges generally parallel the strike of the bounding normal-fault systems (Fig. 1c and d).

The three-dimensional geometry of folds within the Black Mountains accommodation zone, particularly the intersecting anticlines and synclines of disparate trends, is a striking pattern that contrasts with the characteristic style of folding in contractional settings. The trends of the anticlines and synclines locally differ by as much as 90°. This geometry may characterize regional accommodation zones that incorporate the partial along-strike overlap of multiple, oppositely dipping major normal faults. This style of folding occurs at a variety of scales in the Black Mountains accommodation zone. The transversely oriented, east-trending part of the zone in the central Black Mountains (Fig. 3) contains several minor anticlines and synclines that essentially link oppositely dipping normal faults with minimal overlap. Similarly, along-strike overlap between relatively minor, oppositely dipping faults (too small to show on Fig. 4) locally generates minor secondary folds near the tips of the major faults and ends of the larger folds. This probably accounts for the two minor, aforementioned folds in the central Highland Range directly west of the north end of the major anticline. The amplitude, wavelength, and trend of the folds throughout the zone is dependent on the amount of overlap and spacing between the opposing normal-fault systems, as well as the magnitude of extension on each system. Greater overlap and extension produce larger amplitude folds. Variations in the geometric and kinematic parameters of the overlapping, oppositely dipping normal faults can alone generate the disparate orientations of folds within regional accommodation zones.

However, the large stress and strain gradients in regions of overlapping normal faults and fault tips (e.g. Childs et al., 1995; Willemse et al., 1996; Crider and Pollard, 1998; Moore and Schultz, 1999) produce areas of non-plane strain that, in turn, influence the development of fault-related folds in regional accommodation zones. Normal faults in the vicinity of the Highland Range anticline strike northwest in contrast to the predominant northerly striking normal faults in the southeastern Highland Range and elsewhere in the northern Colorado River extensional corridor. Northwest-striking normal faults are also common near the Fire Mountain anticline, which is a major segment of the Black Mountains accommodation zone in the Lake Mohave area (Fig. 3) (Faulds, 1996). Although quantitative modeling of the three-dimensional stress and strain fields in a region of multiple fault tips and overlapping normal faults is beyond the scope of this paper, the above relations imply that the stress and strain fields in such areas are skewed from the regional norm.

The extensional origin of the folds in the Highland Range also has important implications for interpreting the three-dimensional strain field of the Colorado River extensional corridor and possibly for extended terranes in general. The folds within the Highland Range did not result from localized shortening associated with convergence between extensional allochthons above oppositely dipping detachment faults. The lack of reverse faulting and only minor strike-slip faulting within the Highland Range suggest that simultaneous tilting of adjacent fault blocks in opposite directions produced only local structural crowding. These relations may imply that detachment polarity does not flip across the Black Mountains accommodation zone, as Kruger et al. (1998) found across an accommodation zone in central Arizona, or that upper-plate kinematics are more complex than commonly envisioned (e.g. Faulds et al., 1990). Although Tertiary north–south shortening has been documented in the Basin and Range province (e.g. Anderson and Barnhard, 1993), evidence for it has not been observed south of the Lake Mead area. Additionally, the preponderance of north- to northwest-striking normal faults and the trends of the contemporaneous folds in the Highland Range are not compatible with north–south shortening. Instead, the evidence overwhelmingly suggests that the folds in the Highland Range are extensional strain features resulting directly from dip reversals in overlapping, upper-crustal normal-fault systems and corresponding flips in the tilt direction of fault blocks.

5.2. Stratigraphic-structural relations

Both modeling (Ellis and McClay, 1988; McClay, 1989; Xiao and Suppe, 1992) and field studies (e.g. Dorsey and Becker, 1995; Blankenau and Janecke, 1997; Gawthorpe et al., 1997) have shown that extensional folds of various types can significantly affect sedimentation patterns. In particular, the influence of folds within belts of overlapping, oppositely dipping normal-fault systems on sedimentation has been noted in many extended terranes (Scott and Rosendahl, 1989; Morley et al., 1990; Gawthorpe and Hurst, 1993; May and Russell, 1994; Russell and Snelson, 1994; Faulds, 1996). The Highland Range is no exception, as the anticline and syncline both affected depositional patterns of the Miocene volcanic and sedimentary strata.

The central and southeastern Highland Range are distinguished on the basis of stratigraphic and structural variations. Some of the stratigraphic differences can be attributed to lateral variations in volcanic piles associated with proximity to major volcanic centers. However, the distribution of some synextensional units is more likely related to the anticline and syncline. For example, the absence in the central part of the range of the 16.2–16.0 Ma synextensional rhyolites within the volcanics of the Highland Range may be due in part to the topographic high produced by the anticline. The anticline more definitively affected depositional patterns of the synextensional 16.0–15.2 Ma sequence of conglomerate and megabreccia, 15.2 Ma tuff of Bridge Spring, and 15.0 Ma tuff of Mount

Davis. These units are absent from all but the southernmost part of the hinge zone of the southeast-plunging anticline (Fig. 4). Conversely, the thickest sections of the tuffs of Bridge Spring and Mount Davis, as well as the overlying synextensional middle to late Miocene conglomerate, are found near the structurally connected hinge zone of the syncline and west-tilted half graben in the hanging wall of the Highland Pass fault (Figs. 4 and 5), which collectively form the topographic and structural low that separates the central and southeastern domains of the range. Thus, it would appear that the anticline and syncline affected depositional patterns throughout Miocene extension.

The ~16.0–12.8 Ma sedimentary deposits within the Highland Range also record the tectonic and erosional denudation of uplifted footwall blocks. Megabreccias composed of both Proterozoic gneiss and early Miocene intermediate to mafic lavas lie (1) between the 16.0–15.7 Ma upper part of the volcanics of the Highland Range and 15.2 Ma tuff of Bridge Spring, (2) between the tuffs of Bridge Spring and Mount Davis, and (3) within the lower part of the 15.0–12.8 Ma conglomerate (Fig. 8). Thus, the megabreccias began accumulating sometime after about 16.0 Ma and are as young as about 14.5 Ma. The megabreccias are rock-avalanche deposits that represent ancient landslides derived, at least in part, from steep coeval fault scarps. The Proterozoic detritus in both the megabreccias and conglomerate of similar age suggest that the basement rocks of the southern McCullough Range and southern Eldorado Mountains were uplifted and exposed in the footwalls of major normal faults about 16.0 Ma, which coincides with the most rapid rates of tilting. All of these sedimentary units are synextensional growth-fault deposits that accumulated in discrete half grabens and constitute portions of the fold limbs.

Although significant hydrocarbon deposits are unlikely in the northern Colorado River extensional corridor, the extensional folds in the Highland Range may serve as well-exposed analogs of hydrocarbon-rich settings on submerged continental margins. The depositional patterns and geometry and spacing of folds and faults within the Highland Range and elsewhere within the Black Mountains accommodation zone are particularly relevant to exploration analogues. The abundance and spatial association of these extensional folds with severe displacement gradients on major normal faults and the attendant lateral terminations of large half grabens indicate a high probability of structural and stratigraphic closure within regional accommodation zones. It is therefore not surprising that such zones host many substantial oil fields (Morley et al., 1990).

5.3. Nomenclature

A variety of terms have been used to describe folds within zones of overlapping, oppositely dipping normal-fault systems (see discussion in Faulds and Varga, 1998). Although choosing between the terms *accommodation zone* and *transfer zone* for the belts of overlap is somewhat arbitrary (arguments can be made for each), we much prefer a non-genetic, geometric underpinning of the folds within the zones (Faulds and Varga, 1998). The terms *anticlinal* and *synclinal* are helpful, because they convey a clear image of the dominant geometry and are independent of topographic expression or kinematic implications (Fig. 1). Additional modifiers like *oblique* and *strike-parallel* further depict the geometry of the folds, relative to the strike of the dominant set of normal faults, in a non-genetic manner. These terms are more widely applicable than names such as *high-* and *low-relief* (Rosendahl, 1987) and *interference* and *isolational* (Scott and Rosendahl, 1989). For example, the extensional anticline in the Highland Range, which is a low-relief zone in the nomenclature of Rosendahl (1987), is actually a topographic high, whereas the extensional syncline (high-relief zone of Rosendahl, 1987) constitutes a topographic low. The word interference (Scott and Rosendahl, 1989) is also potentially misleading, as the amount of interference between oppositely tilted fault blocks is dependent on both the relative timing of deformation and regional kinematics. As in the Highland Range, the actual interference or structural crowding between the opposing limbs of the folds may be minimal. Similarly, the terms anticlinal and synclinal are favored over the terms *convergent* and *divergent* (Morley et al., 1990), because they cannot be construed as implying relative translations or types of strain within an accommodation zone (e.g. convergent could imply contractional strain, although Morley et al. (1990) did not use it in this way). Thus, we classify the folds in the Highland Range as oblique anticlinal and synclinal accommodation zones (Fig. 1).

6. Conclusions

The Black Mountains accommodation zone, spanning the highly extended northern Colorado River extensional corridor of the Basin and Range province, contains several interconnected anticlines and synclines. These folds are defined by thick sections of Miocene volcanic and sedimentary strata that accumulated immediately prior to and during regional extension. The westernmost anticline and syncline lie within the Highland Range and are interpreted as fault-related, extensional folds produced by the partial along-strike overlap of oppositely dipping normal-fault systems and attendant tilt-block domains. The west-tilted limbs of the folds are dominated by east-dipping normal faults, whereas west-dipping normal faults characterize the east-tilted limbs. Consistent crosscutting relationships were not observed between the opposing normal-fault sets. In the Highland Range, the northwest-trending anticline terminates northward near the tip of the east-dipping McCullough Range normal fault and ends southward at the intersection with the northeast-trending syncline. The anticline was generated by the intersection of opposing rollovers

developed in the hanging walls of oppositely dipping normal faults that dip toward one another and overlap along strike, mainly the east-dipping McCullough Range and west-dipping Keyhole Canyon faults. The syncline developed between overlapping, outwardly dipping listric faults, as adjacent fault blocks were tilted toward one another, possibly through a combination of reverse drag and footwall uplift. The regional syncline merges with a smaller amplitude, hanging wall syncline developed near the tip of a major normal fault before terminating at the intersection with the anticline. The geometry of the folds is open, generally symmetrical, and parallel, with subhorizontal hingelines and steeply inclined to upright axial surfaces. The folds were produced primarily by fault-bend folding, but drag-folding, displacement-gradient folding, and fault-propagation folding played subsidiary roles.

The limbs of the folds merge into and comprise parts of major half grabens. Tilt fanning within these half grabens and 15 new $^{40}Ar/^{39}Ar$ dates bracket major extension between about 16.5 and 11 Ma, which coincides with major extension in much of the northern Colorado River extensional corridor. Tilting of the opposing fold limbs was synchronous. The anticline and syncline significantly affected depositional patterns, with synextensional units, including two major ash-flow tuffs, thinning toward the anticlinal hinge and thickening toward the synclinal hinge.

Folding in the Highland Range cannot be attributed to localized shortening associated with convergence between extensional allochthons above oppositely dipping detachment faults, as evidenced by a preponderance of normal faults and lack of reverse faults. Minor strike-slip faulting within the hinge zone of the anticline suggests only localized structural crowding between adjacent, oppositely tilted fault blocks.

Northwest-striking normal faults dominate the Highland Range anticline in contrast to more northerly striking normal faults elsewhere in the northern Colorado River extensional corridor. This suggests a slight reorientation of stress and strain fields in the zone of overlapping normal faults and fault tips near the anticline.

Acknowledgements

Field and laboratory work were supported by two National Science Foundation grants (EAR93-16770 and EAR98-96032) awarded to Faulds and a grant from the U.S. Geological Survey STATEMAP Program (Agreement No. HQ-AG-2036). The views and conclusions contained in this document are, however, those of the authors and should not be interpreted as necessarily representing the official policies, either expressed or implied, of the U.S. Government. Constructive reviews by Ted Apotria, Stefan Boettcher, and Jon Spencer greatly improved this manuscript. We owe substantial thanks to the hospitality of Barney and Elaine Reagan during this study. The National Park Service at the Lake Mead National Recreation Area provided housing during several field stints, for which we thank Kent Turner, Glenn Anderson, and Darlene Carnes. We also thank Gary Dixon and Pete Rowley of the U.S. Geological Survey for providing a field vehicle for part of this study. We have benefited from fruitful discussions with Robert Varga, Calvin Miller, Eugene Smith, and Daniel Feuerbach.

References

Anderson, R.E., 1971. Thin skin distension in Tertiary rocks of southeastern Nevada. Geological Society of America Bulletin 82, 43–58.

Anderson, R.E., 1977. Geologic map of the Boulder City 15-minute Quadrangle, Clark County, Nevada. U.S. Geological Survey Geologic Quadrangle Map GQ-1395, scale 1:62,500.

Anderson, R.E., 1978. Geologic map of the Black Canyon 15-minute Quadrangle, Mohave County, Arizona and Clark County, Nevada. U.S. Geological Survey Geologic Quadrangle Map GQ-1394, scale 1:62,500.

Anderson, R.E., Barnhard, T.P., 1993. Aspects of three-dimensional strain at the margin of the extensional orogen, Virgin River depression area, Nevada, Utah, and Arizona. Geological Society of America Bulletin 105, 1019–1052.

Anderson, R.E., Longwell, C.R., Armstrong, R.L., Marvin, R.F., 1972. Significance of K–Ar ages of Tertiary rocks from the Lake Mead region, Nevada–Arizona. Geological Society of America Bulletin 83, 273–288.

Anderson, R.E., Barnhard, T.P., Snee, L.W., 1994. Roles of plutonism, midcrustal flow, tectonic rafting, and horizontal collapse in shaping the Miocene strain field of the Lake Mead area, Nevada and Arizona. Tectonics 13, 1381–1410.

Angelier, J., Colletta, B., Anderson, R.E., 1985. Neogene paleostress changes in the Basin and Range; a case study at Hoover Dam, Nevada–Arizona. Geological Society of America Bulletin 96, 347–361.

Bachl, C.A., 1997. The Searchlight pluton: an example of wholesale magmatic reconstruction of the upper crust during continental extension. M.S. thesis, Vanderbilt University.

Bingler, E.C., Bonham, H.F., Jr., 1973. Reconnaissance geologic map of the McCullough Range and adjacent areas, Clark County, Nevada. Nevada Bureau of Mines and Geology Map 45, scale 1:25,000.

Blankenau, J.J., Janecke, S.U., 1997. Three-dimensional structure of a Paleogene rift basin and its effects on synextensional sedimentation, Salmon basin, ID. Geological Society of American Abstracts with Programs 29, 221.

Campbell, E.A., John, B.E., 1996. Constraints on extension-related plutonism from modeling of the Colorado River gravity high. Geological Society of America Bulletin 108, 1242–1255.

Childs, C., Watterson, J., Walsh, J.J., 1995. Fault overlap zones within developing normal fault systems. Journal of the Geological Society of London 152, 535–549.

Colletta, B., Le Quellec, P., Letouzey, J., Moretti, I., 1988. Longitudinal evolution of the Suez rift structure (Egypt). In: Le Pichon, X., Cochran, J.R. (Eds.), The Gulf of Suez and Red Sea Rifting. Tectonophysics 153, 221–233.

Crider, J.G., Pollard, D.D., 1998. Fault linkage: three-dimensional mechanical interaction between echelon normal faults. Journal of Geophysical Research 103, 24,373–24,391.

Dalrymple, G.B., Lanphere, M.A., 1969. Potassium–Argon Dating. W.H. Freeman Company, New York.

Darvall, P., 1991. Miocene extension and volcanism in the Eldorado Mountains, southeast Nevada, USA. M.S. thesis, Monash University.

Davis, G.A., Lister, G.S., 1988. Detachment faulting in continental exten-

sion: perspectives from the southwestern U.S. Cordillera. Geological Society of American Special Paper 218, 133–159.

Davis, G.A., Anderson, J.L., Frost, E.G., Shackelford, T.J., 1980. Mylonitization and detachment faulting in the Whipple–Buckskin–Rawhide Mountains terrane, southeastern California and western Arizona. In: Crittenden, M.D., Coney, P.J., Davis, G.H. (Eds.), Cordilleran Metamorphic Core Complexes. Geological Society of America Memoir 153, 79–130.

Davis, S.O., 1984. Structural geology of the central part of the Highland Spring Range, Clark County, Nevada. M.S. thesis, University of Southern California.

Deino, A., Potts, R., 1990. Single-crystal $^{40}Ar/^{39}Ar$ dating of the Olorgesailie Formation, Southern Kenya Rift. Journal of Geophysical Research 95, 8453–8470.

Deino, A., Potts, R., 1992. Age-probability spectra from examination of single-crystal $^{40}Ar/^{39}Ar$ dating results: examples from Olorgesailie, Southern Kenya Rift. Quaternary International 13/14, 47–53.

DeWitt, E., Anderson, J.L., Barton, H.N., Jachens, R.C., Podwysocki, M.H., Brickey, D.W., Close, T.J., 1989. Mineral resources of the South McCullough Mountains Wilderness Study Area, Clark County, Nevada. U.S. Geological Survey Bulletin 1730-C.

Dorsey, R.J., Becker, U., 1995. Evolution of a large Miocene growth structure in the upper plate of the Whipple detachment fault, northeastern Whipple Mountains, California. Basin Research 7, 151–163.

Duebendorfer, E.M., Wallin, E.T., 1991. Basin development and synteclonic sedimentation associated with kinematically couple strike-slip and detachment faulting, southern Nevada. Geology 19, 87–90.

Duebendorfer, E.M., Sharp, W.D., 1998. Variation in displacement along strike of the South Virgin–White Hills detachment fault: perspective from the northern White Hills, northwestern Arizona. Geological Society of America Bulletin 110, 1574–1589.

Duebendorfer, E.M., Sewall, A.J., Smith, E.I., 1990. The Saddle Island detachment; an evolving shear zone in the Lake Mead area, Nevada. In: Wernicke, B.P. (Ed.), Basin and Range Extensional Tectonics Near the Latitude of Las Vegas, Nevada. Geological Society of America Memoir 176, 77–98.

Dula, W.F., 1991. Geometric models of listric normal faults and rollover folds. American Association of Petroleum Geologists Bulletin 75, 1609–1625.

Ebinger, C.J., 1989. Geometric and kinematic development of border faults and accommodation zones, Kivu–Rusizi rift, Africa. Tectonics 8, 117–133.

Ellis, P.G., McClay, K.R., 1988. Listric extensional fault systems — results of analogue model experiments. Basin Research 1, 55–70.

Etheridge, M.A., Symonds, P.A., Powell, T.G., 1988. Application of the detachment model for continental extension to hydrocarbon exploration in extensional basins. Australian Petroleum Exploration Association Journal 28, 167–187.

Faulds, J.E., 1994. New insights on the geometry and kinematics of the Black Mountains–Highland Spring Range accommodation zone (BHZ), Arizona and Nevada. Geological Society of America Abstracts with Programs 26, 51.

Faulds, J.E., 1995. Geologic map of the Mount Davis Quadrangle, Nevada and Arizona. Nevada Bureau of Mines and Geology Map 105, scale 1:24,000.

Faulds, J.E., 1996. Geologic map of the Fire Mountain Quadrangle, Nevada and Arizona. Nevada Bureau of Mines and Geology Map 106, scale 1:24,000.

Faulds, J.E., Olson, E.L., 1997. Implications of paleomagnetic data on 3-D strain accommodation related to displacement gradients on major normal faults. Geological Society of America Abstracts with Programs 29, 375.

Faulds, J.E., Varga, R.J., 1998. The role of accommodation zones and transfer zones in the regional segmentation of extended terranes. In: Faulds, J.E., Stewart, J.H. (Eds.), Accommodation Zones and Transfer Zones: The Regional Segmentation of the Basin and Range Province. Geological Society of America Special Paper 323, 1–46.

Faulds, J.E., Bell, J.W., 1999. Geologic map of the Nelson SW Quadrangle, Clark County, Nevada. Nevada Bureau of Mines and Geology Open-File Report 99-15, scale 1:24,000.

Faulds, J.E., Geissman, J.W., Mawer, C.K., 1990. Structural development of a major extensional accommodation zone in the Basin and Range province, northwestern Arizona and southern Nevada. In: Wernicke, B.P. (Ed.), Basin and Range Extensional Tectonics Near the Latitude of Las Vegas, Nevada. Geological Society of America Memoir 176, 37–76.

Faulds, J.E., Geissman, J.W., Shafiqullah, M., 1992. Implications of paleomagnetic data on Miocene extension near a major accommodation zone in the Basin and Range province, northwestern Arizona and southern Nevada. Tectonics 11, 204–227.

Faulds, J.E., Gans, P., Smith, E.I., 1994. Spatial and temporal patterns of extension in the northern Colorado River extensional corridor, northwestern Arizona and southern Nevada. Geological Society of America Abstracts with Programs 26, 51.

Faulds, J.E., Feuerbach, D.L., Reagan, M.K., Metcalf, R.V., Gans, P., Walker, J.D., 1995. The Mount Perkins block, northwestern Arizona: An exposed cross-section of an evolving, preextensional to synextensional magmatic system. Journal of Geophysical Research 100, 15,249–15,266.

Faulds, J.E., Shaw, M., Miller, C.F., 1996. Progressive development of metamorphic core complexes and detachment faults, Colorado River extensional corridor, western USA. Geological Society of America Abstracts with Programs 28, 511.

Faulds, J.E., Miller, C.F., Bachl, C.A., Ruppert, R., Heizler, M., 1998. Emplacement of thick Miocene magmatic crust, Eldorado Mountains, Nevada: Pre-extensional (?) crustal mass transfer in the Basin and Range. EOS (Abstract), American Geophysical Union 79, 565.

Faulds, J.E., Smith, E.I., Gans, P., 1999. Spatial and temporal patterns of magmatism and extension in the northern Colorado River extensional corridor, Nevada and Arizona: a preliminary report. Nevada Petroleum Society Guidebook 14, 171–183.

Feuerbach, D.L., Faulds, J.E., Reagan, M.K., 1999. Interrelations between magmatism and extension in a major accommodation zone, southern Nevada and northwest Arizona. Nevada Petroleum Society Guidebook 14, 115–138.

Flannery, J.W., Rosendahl, B.R., 1990. The seismic stratigraphy of Lake Malawi, Africa: implications for interpreting geological processes in lacustrine rifts. Journal of African Earth Sciences 10, 519–548.

Fleck, R.J., Sutter, J.F., Elliott, D.H., 1977. Interpretation of discordant $^{40}Ar/^{39}Ar$ age spectra of Mesozoic tholeiites from Antarctica. Geochimica Cosmochim Acta 41, 15–32.

Fleuty, M.J., 1964. The description of folds. Geological Association Proceedings 75, 461–492.

Fryxell, J.E., Salton, C.G., Selverstone, J., Wernicke, B., 1992. Gold Butte crustal section, South Virgin Mountains, Nevada. Tectonics 11, 1099–1120.

Gans, P.B., Bohrson, W.A., 1998. Suppression of volcanism during rapid extension in the Basin and Range province, United States. Science 279, 66–68.

Gans, P.B., Mahood, G.A., Schermer, E., 1989. Synextensional magmatism in the Basin and Range province; a case study in the eastern Great Basin. Geological Society of America Special Paper, 233.

Gans, P.B., Landau, B., Darvall, P., 1994. Ashes, ashes, all fall down: Caldera-forming eruptions and extensional collapse of the Eldorado Mountains, southern Nevada. Geological Society of America Abstracts with Programs 26, 53.

Gawthorpe, R.L., Hurst, J.M., 1993. Transfer zones in extensional basins: their structural style and influence on drainage development and stratigraphy. Geological Society of London Journal 150, 1137–1152.

Gawthorpe, R.L., Sharp, I., Underhill, J.R., Gupta, S., 1997. Linked sequence stratigraphic and structural evolution of propagating normal faults. Geology 25, 795–798.

Glazner, A.F., Bartley, J.M., 1984. Timing and tectonic setting of Tertiary

low-angle normal faulting and associated magmatism in the southwestern United States. Tectonics 3, 385–396.

Glazner, A.F., Nielson, J.E., Howard, K.A., Miller, D.M., 1986. Correlation of the Peach Spring Tuff, a large-volume Miocene ignimbrite sheet in California and Arizona. Geology 14, 840–843.

Groshong Jr, R.J., 1989. Half-graben structures: balanced models of extensional fault-bend folds. Geological Society of America Bulletin 101, 96–105.

Groshong Jr, R.J., 1994. Area balance, depth to detachment, and strain in extension. Tectonics 13, 1488–1497.

Hamblin, W.K., 1965. Origin of 'reverse drag' on the downthrown side of normal faults. Geological Society of America Bulletin 76, 1145–1165.

Howard, K.A., John, B.E., 1987. Crustal extension along a rooted system of imbricate low-angle faults; Colorado River extensional corridor, California and Arizona. In: Coward, M.P., Dewey, J.F., Hancock, P.L. (Eds.), Continental Extensional Tectonics. Geological Society Special Publication 28, 299–311.

Janecke, S.U., Vandenberg, C.J., Blankenau, J.J., 1998. Geometry, mechanism, and significance of extensional folds from examples in the Rocky Mountain Basin and Range province, USA. Journal of Structural Geology 20, 841–856.

John, B.E., Foster, D.A., 1993. Structural and thermal constraints on the initiation angle of detachment faulting in the southern Basin and Range: The Chemehuevi Mountains case study. Geological Society of America Bulletin 105, 1091–1108.

Kruger, J.M., Faulds, J.E., Reynolds, S.J., Okaya, D.A., 1998. Seismic reflection evidence for detachment polarity beneath a major accommodation zone, west-central Arizona. In: Faulds, J.E., Stewart, J.H. (Eds.), Accommodation Zones and Transfer Zones: The Regional Segmentation of the Basin and Range Province. Geological Society of America Special Paper 323, 89–114.

Mahon, K.I., 1996. The New "York" regression: application of an improved statistical method to geochemistry. International Geology Review 38, 293–303.

May, S.J., Russell, L.R., 1994. Thickness of the syn-rift Santa Fe Group in the Albuquerque basin and its relation to structural style. In: Keller, G.R., Cather, S.M. (Eds.), Basins of the Rio Grande rift: Structure, Stratigraphy, and Tectonic Setting. Geological Society of America Special Paper 291, 113–123.

McClay, K.R., 1989. Physical models of structural styles during extension. In: Tankard, A.J., Balkwill, H.R. (Eds.), Extensional Tectonics and Stratigraphy of the North Atlantic Margins. American Association of Petroleum Geologists Memoir 46, 95–110.

Miller, C.F., Bachl, C.A., Miller, J.S., Wooden, J.L., Faulds, J.E., Shaw, M.L., 1995. Mid-crustal plutons of the Eldorado Mountains: evidence for large-scale magmatic modification and reorganization of the crust in the Colorado River extensional corridor. Geological Society of America Abstracts with Programs 27, 435.

Miller, C.F., Faulds, J.E., Bachl, C.A., Ruppert, R., 1998. Searchlight pluton, Eldorado Mountains, Nevada: massive pluton emplacement at the onset of continental extension. EOS (Abstract), American Geophysical Union 79, 342–343.

Moore, J.M., Schultz, R.A., 1999. Processes of faulting in jointed rocks of Canyonlands National Park, Utah. Geological Society of America Bulletin 111, 808–822.

Morikawa, S.A., 1994. The geology of the tuff of Bridge Spring, southern Nevada and northwestern Arizona. M.S. thesis, University of Nevada, Las Vegas.

Morley, C.K., Nelson, R.A., Patton, T.L., Munn, S.G., 1990. Transfer zones in the East African Rift system and their relevance to hydrocarbon exploration in rifts. American Association of Petroleum Geologists Bulletin 74, 1234–1253.

Nielson, J.E., Lux, D.R., Dalrymple, G.B., Glazner, A.F., 1990. Age of the Peach Springs Tuff, southeastern California and western Arizona. Journal of Geophysical Research 95, 571–580.

Olson, E.L., 1996. Geometry and kinematics of an extensional anticline, Highland Spring Range, southern Nevada. M.S. thesis, University of Iowa.

Patton, T.L., Moustafa, A.R., Nelson, R.A., Abdine, S.A., 1994. Tectonic evolution and structural setting of the Suez rift. In: Landon, S.M. (Ed.), Interior Rift Basins. American Association of Petroleum Geologists Memoir 59, 9–55.

Price, L.M., Faulds, J.E., 1999. Structural development of a major segment of the Colorado Plateau–Basin and Range boundary, southern White Hills, Arizona. Nevada Petroleum Society Guidebook 14, 139–170.

Proffett Jr, J.M., 1977. Cenozoic geology of the Yerington district, Nevada, and implications for the nature and origin of Basin and Range faulting. Geological Society of America Bulletin 88, 247–266.

Ramsay, J.G., 1967. Folding and Fracturing of Rocks. McGraw-Hill Book Company, New York.

Rosendahl, B.R., 1987. Architecture of African rifts with special reference to East Africa. Annual Review Earth and Planetary Science 15, 445–503.

Ruppert, R.F., 1999. Structural and stratigraphic framework of the northern Newberry Mountains, southern Nevada: assessing the interplay between magmatism and extension. M.S. thesis, University of Iowa.

Ruppert, R.F., Faulds, J.E., Miller, C.F., Heizler, M., 1999. Interplay between magmatism and N–S and E–W extension, northern Newberry Mountains, southern Nevada. Geological Society of America Abstracts with Programs 31, 90.

Russell, L.R., Snelson, S., 1994. Structure and tectonics of the Albuquerque Basin segment of the Rio Grande rift: insights from reflection seismic data. In: Keller, G.R., Cather, S.M. (Eds.), Basins of the Rio Grande Rift: Structure, Stratigraphy, and Tectonic Setting. Geological Society of America Special Paper 291, 83–112.

Samson, S.D., Alexander Jr, E.C., 1987. Calibration of the interlaboratory standard MMhb-1. Chemical Geology 66, 27–34.

Schlische, R.W., 1992. Structural and stratigraphic development of the Newark extensional basin, eastern North America: evidence for the growth of the basin and its bounding structures. Geological Society of America Bulletin 104, 1246–1263.

Schlische, R.W., 1993. Anatomy and evolution of the Triassic–Jurassic continental rift system, eastern North America. Tectonics 12, 1026–1042.

Schlische, R.W., 1995. Geometry and origin of fault-related folds in extensional settings. American Association of Petroleum Geologists Bulletin 79, 1661–1678.

Scott, D.L., Rosendahl, B.R., 1989. North Viking graben: an East African perspective. American Association of Petroleum Geologists Bulletin 73, 155–165.

Smith, E.I., Faulds, J.E., 1994. Patterns of Miocene magmatism in the northern Colorado River extensional corridor (NCREC), Nevada, Arizona and California. Geological Society of America Abstracts with Programs 26, 93.

Spencer, J.E., 1984. Role of tectonic denudation in warping and uplift of low-angle normal faults. Geology 12, 95–98.

Spencer, J.E., 1985. Miocene low-angle normal faulting and dike emplacement, Homer Mountain and surrounding areas, southeastern California and southernmost Nevada. Geological Society of America Bulletin 96, 1140–1155.

Spencer, J.E., Reynolds, S.J., 1989. Middle Tertiary tectonics of Arizona and adjacent areas. In: Jenney, J.P., Reynolds, S.J. (Eds.), Geologic Evolution of Arizona. comment > Arizona Geological Society Digest 17, 539–574.

Steiger, R.H., Jäeger, E., 1977. Subcommission on geochronology: convention on the use of decay constants in geo- and cosmochronology. Earth and Planetary Science Letters 36, 359–362.

Stewart, J.H., 1980. Regional tilt pattern of late Cenozoic Basin–Range fault blocks, western United States. Geological Society of America Bulletin 91, 460–464.

Suppe, J., 1985. Principles of Structural Geology. Prentice Hall, Englewood Cliffs, New Jersey.

Taylor, J.R., 1997. An Introduction to Error Analysis: The Study of Uncertainties in Physical Measurements. 2nd Ed University Science Books, Mill Valley.

Turner, R.D., Glazner, A.F., 1990. Miocene volcanism, folding, and faulting in the Castle Mountains, southern Nevada and eastern California. In: Wernicke, B.P. (Ed.), Basin and Range Extensional Tectonics Near the Latitude of Las Vegas, Nevada. Geological Society of America Memoir 176, 23–36.

Varga, R.J., Faulds, J.E., Harlan, S.S., 1996. Regional extent and dominant geometry of the Black Mountains accommodation zone, northwest Arizona and southern Nevada. Geological Society of America Abstracts with Programs 28, 512.

Weber, M.E., Smith, E.I., 1987. Structural and geochemical constraints on the reassembly of disrupted mid-Miocene volcanoes in the Lake Mead–Eldorado Valley area of southern Nevada. Geology 15, 553–556.

Wernicke, B., 1985. Uniform-sense normal simple shear of the continental lithosphere. Canadian Journal of Earth Sciences 22, 108–125.

Wernicke, B., Axen, G.J., 1988. On the role of isostasy in the evolution of normal fault systems. Geology 4, 848–851.

Willemse, E.J., Pollard, D.D., Aydin, A., 1996. Three-dimensional analyses of slip distributions on normal fault arrays with consequences for fault scaling. Journal of Structural Geology 18, 295–309.

Xiao, H., Suppe, J., 1992. Origin of rollover. American Association of Petroleum Geologists Bulletin 76, 509–529.

Yarnold, J.C., Lombard, J.P., 1989. A facies model for large rock-avalanche deposits formed in dry climates. In: Colburn, I.P., Abbott, P.L., Minch, J. (Eds.), Conglomerates in Basin Analysis: A Symposium Dedicated to A.O. Woodward. Pacific Section of Society of Economic Paleontologists and Mineralogists 62, 9–31.

Yin, A., Dunn, J.F., 1992. Structural and stratigraphic development of the Whipple–Chemehuevi detachment fault system, southeastern California: Implications for the geometrical evolution of domal and basinal low-angle normal faults. Geological Society of America Bulletin 104, 659–674.